Quaternary Science Reviews 158 (2017) 58–76

Contents lists available at ScienceDirect

Quaternary Science Reviews

journal homepage: www.elsevier.com/locate/quascirev

Deglacial history of the Pensacola Mountains, Antarctica from glacial geomorphology and cosmogenic nuclide surface exposure dating

M.J. Bentley [a, *], A.S. Hein [b], D.E. Sugden [b], P.L. Whitehouse [a], R. Shanks [c], S. Xu [c], S.P.H.T. Freeman [c]

[a] Department of Geography, Durham University, Lower Mountjoy, South Rd, Durham, DH1 3LE, UK
[b] School of Geosciences, University of Edinburgh, Drummond St, Edinburgh, EH8 9XP, UK
[c] AMS Laboratory, Scottish Universities Environmental Research Centre, Scottish Enterprise Technology Park, East Kilbride, G75 0QF, UK

ARTICLE INFO

Article history:
Received 22 April 2016
Received in revised form
20 September 2016
Accepted 27 September 2016

Keywords:
Antarctica
Cosmogenic isotopes
Glacial geomorphology
Ice sheet history

ABSTRACT

The retreat history of the Antarctic Ice Sheet is important for understanding rapid deglaciation, as well as to constrain numerical ice sheet models and ice loading models required for glacial isostatic adjustment modelling. There is particular debate about the extent of grounded ice in the Weddell Sea embayment at the Last Glacial Maximum, and its subsequent deglacial history. Here we provide a new dataset of geomorphological observations and cosmogenic nuclide surface exposure ages of erratic samples that constrain the deglacial history of the Pensacola Mountains, adjacent to the present day Foundation Ice Stream and Academy Glacier in the southern Weddell Sea embayment. We show there is evidence of at least two glaciations, the first of which was relatively old and warm-based, and a more recent cold-based glaciation. During the most recent glaciation ice thickened by at least 450 m in the Williams Hills and at least 380 m on Mt Bragg. Progressive thinning from these sites was well underway by 10 ka BP and ice reached present levels by 2.5 ka BP, and is broadly similar to the relatively modest thinning histories in the southern Ellsworth Mountains. The thinning history is consistent with, but does not mandate, a Late Holocene retreat of the grounding line to a smaller-than-present configuration, as has been recently hypothesized based on ice sheet and glacial isostatic modelling. The data also show that clasts with complex exposure histories are pervasive and that clast recycling is highly site-dependent. These new data provide constraints on a reconstruction of the retreat history of the formerly-expanded Foundation Ice Stream, derived using a numerical flowband model.

1. Background and rationale

The Antarctic Ice Sheet is the largest potential contributor to future sea-level rise. It is currently losing mass (King et al., 2012; Shepherd et al., 2012) and some studies suggest that the rate of mass loss is accelerating (Harig and Simons, 2015; Velicogna et al., 2014; Williams et al., 2014). Understanding the past history of the ice sheet is important because: it can inform how the ice sheet has responded to past environmental changes, and record its trajectory preceding the observational record; it allows us to test ice sheet models by hindcasting; and it provides us with inputs for models of glacial isostatic adjustment (GIA), which are needed to interpret satellite gravimetric measurements of ice mass loss (Bentley, 2010).

The Weddell Sea sector of the ice sheet has not seen the same level of attention as other areas such as the Amundsen Sea and Ross Sea. This is despite some studies suggesting that the area is particularly susceptible to ice shelf thinning (Hellmer et al., 2012) and grounding line retreat (Ross et al., 2012; Wright et al., 2014). Part of this sensitivity derives from the fact that the southern part of the area is overdeepened, particularly in the east, where several subglacial basins are comparable in depth to other deep but grounded parts of the West Antarctic Ice Sheet, for example, along the Amundsen Sea coast. The largest trough in the Weddell Sea, the Foundation-Thiel Trough, is 1300–1500 m deep and extends north-south for >1000 km, right across the Weddell Sea continental shelf to the shelf break (Fig. 1). Its position, size and extent mean that it was once occupied by a major ice stream (the “Thiel Trough Ice Stream”) draining ice through an area east of Berkner Island. This ice stream is likely to have exerted a key control on regional ice elevation.

* Corresponding author.
E-mail address: m.j.bentley@durham.ac.uk (M.J. Bentley).

http://dx.doi.org/10.1016/j.quascirev.2016.09.028

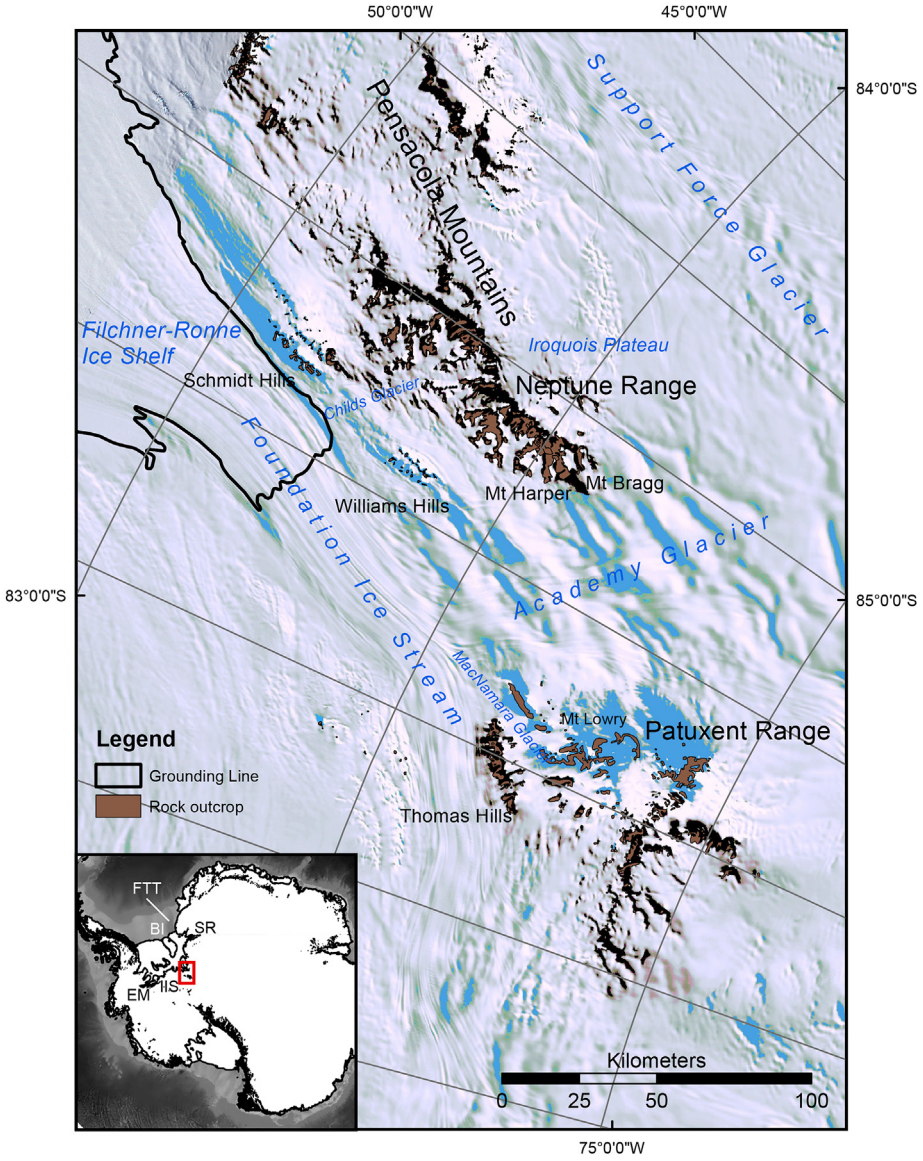

Fig. 1. Location Map of the Pensacola Mountains study area, adjacent to the Foundation Ice Stream and its tributary the Academy Glacier. Background is Landsat imagery from the LIMA mosaic. Rock outcrop and grounding line are from Antarctic Digital Database. Bathymetry is from BEDMAP2 (Fretwell et al., 2013). Inset shows location within the southern Weddell Sea embayment. BI=Berkner Island; EM = Ellsworth Mountains; FTT=Foundation-Thiel Trough; IIS=Institute Ice Stream; SR=Shackleton Range.

At present there are two alternative models for the Last Glacial Maximum (LGM) extent of ice in the Weddell Sea embayment (Bentley et al., 2014; Hillenbrand et al., 2014). The first, based largely on marine geological evidence is an extensive model with ice grounded over the outer continental shelf (Hillenbrand et al., 2012; Larter et al., 2012). The implication of this model is that the Thiel Trough Ice Stream would be grounded as far as the shelf break. The second, based largely on terrestrial evidence of minor elevational change of the ice sheet at the LGM (Bentley et al., 2010; Hein et al., 2011; Mulvaney et al., 2007) is a restricted model with the grounding line of the Thiel Trough Ice Stream confined to the mid- to inner-shelf (Bentley et al., 2010; Hillenbrand et al., 2014; Le Brocq et al., 2011; Whitehouse et al., 2012).

In addition to the debate on ice sheet extent, the timing of post-glacial thinning in the Weddell Sea is not yet well understood. This hampers the development of ice loading models for GIA modelling, and the understanding of recent (Late Holocene) change in the region. For example, although most studies have assumed a simple retreat from LGM to present, a recent study has demonstrated that a Late Holocene re-advance of the ice sheet may explain some formerly puzzling observations from GPS and glaciological surveys (Bradley et al., 2015). Such a readvance has important implications for our understanding of ice sheet stability, in that it implies that some grounding lines on inward dipping bedrock beds may be advancing (Bradley et al., 2015). Such 'unstable advance' has been suggested on theoretical grounds (Schoof, 2007). We require further observational data on ice sheet retreat timing to test the validity of such ideas.

Our aim in this paper is to determine former ice sheet extent and elevation change adjacent to the southern extension of the Thiel Trough Ice Stream (Fig. 1). The glacial geology of this area contains a record of ice thickness change that can yield information on the extent of ice along the Foundation-Thiel Trough, and the timing of its thinning from the local last glacial maximum (LLGM) (Clark et al., 2009) to its present configuration. This paper describes the geomorphological evidence of former thicker ice levels in the

northern Pensacola Mountains and then provides a chronology of deglacial ice sheet thinning using cosmogenic nuclide surface exposure dating. We also compare our results to a study of similar sites in the Pensacola Mountains (Balco et al., 2016). A companion paper to this one (Whitehouse et al., 2016) uses a glaciological model to explore the implications of the data presented both here and in Balco et al. (2016) with regard to the former extent of ice in the Foundation-Thiel Trough.

2. Study area and methods

The study area is the northern Pensacola Mountains, located at the southern extension of the Foundation-Thiel Trough (Fig. 1). The Pensacola Mountains are split into the Neptune Range in the north, and the Patuxent Range in the south. The Foundation Ice Stream, fed by the tributary Academy Glacier, flows south to north through the area and becomes afloat close to the Schmidt Hills. The Foundation Ice Stream is by far the largest West Antarctic Ice Sheet outlet in the south-eastern Weddell Sea: indeed today it contributes more ice to the Weddell embayment than any other outlet except the Evans Ice Stream (Joughin and Bamber, 2005). The margins of the Academy Glacier and Foundation Ice Stream have several blue-ice areas with abundant supraglacial morainic debris, and this coupled to the presence of numerous nunataks along their flanks means that there is a rich record of past ice sheet elevational changes preserved.

We studied the geomorphology and sampled altitudinal transects of erratic sandstone clasts at several sites: Schmidt Hills, Williams Hills, Mt. Bragg and Mt. Harper, and Thomas Hills (Figs. 1 and 2.). Striation directions are corrected to true north using declination values that vary across the study area from 23 to 31° east of north.

2.1. Sampling of erratics and cosmogenic nuclide analysis

The geology of the Pensacola Mountains is dominated by quartz-bearing lithologies: dominantly a mix of folded sandstones, mudstones, conglomerates and limestones, with a more minor series of lava flows and pillow lavas in the western part (Schmidt et al., 1978) and so a large proportion of erratics are suitable for exposure dating using ^{10}Be and ^{26}Al contained in quartz. The presence of abundant erratics left behind by a thinning ice sheet was noted by Schmidt et al. (1978) who described erratics on 'most rock slopes' up to 1000 m above present day ice. Erratic samples were taken whole or sampled from larger boulders with a hammer and chisel. Our particular focus was in understanding the deglacial (thinning) history of the different areas studied and we sampled erratics along altitudinal transects for this reason. The sampling strategy for cosmogenic nuclides was designed to reduce the chance of nuclide inheritance, and exclude the possibility of nuclide loss through erosion. Specifically, we sampled erratics that were perched on bedrock, felsenmeer or drift surfaces, and avoided any samples that were embedded in drift, or sitting at the base of slopes in order to minimise problems of post-depositional movement and self-shielding. Because our focus is on the most recent deglacial thinning we selected the freshest erratics, and so avoided erratics with weathering such as ventification, tafoni, spallation, weathering rinds or patina. We targeted sub-glacially derived clasts with striated surfaces and sub-angular to sub-rounded shapes. Topographic shielding was measured using an abney level and compass.

The sample and cosmogenic nuclide data are presented in Tables 1 and 2, and Fig. 2. All exposure ages discussed are based on ^{10}Be ages because the production rate is better constrained; ^{26}Al was used to provide a check on a range of selected samples from different sites and in particular to determine, within the errors of the approach, that the younger ages were concordant within error - and therefore less likely to be reworked. In the case of the older ages (>100 ka) we used ^{26}Al analysis of a sub-set of samples to determine whether they had experienced periods of burial, and were therefore more likely to record complex exposure histories or reworking over more than one interval of ice sheet thickening and thinning.

2.2. Laboratory and analytical techniques

Whole rock samples were crushed and sieved to obtain the 250–710 μm fraction. Be and Al were selectively extracted from the quartz component of the whole-rock sample at the University of Edinburgh's Cosmogenic Nuclide Laboratory following established methods (Bierman et al., 2002; Kohl and Nishiizumi, 1992). ^{10}Be/^{9}Be and ^{26}Al/^{27}Al ratios were measured in 20–30 g of quartz at the Scottish Universities Environmental Research Centre (SUERC) Accelerator Mass Spectrometry (AMS) Laboratory in East Kilbride, UK. Measurements are normalised to the NIST SRM-4325 Be standard material with a revised (Nishiizumi et al., 2007) nominal ^{10}Be/^{9}Be of 2.79×10^{-11}, and the Purdue Z92-0222 Al standard material with a nominal ^{26}Al/^{27}Al of 4.11×10^{-11}, which agrees with the Al standard material of Nishiizumi (2004) with half-life of 0.705 Ma (Xu et al., 2010). SUERC ^{10}Be-AMS is insensitive to ^{10}B interference (Xu et al., 2013) and the interferences to ^{26}Al detection are well characterised (Xu et al., 2014). Process blanks (n = 19) and samples were both spiked with 250 μg ^{9}Be carrier (Scharlau Be carrier, 1000 mg/l, density 1.02 g/ml). Blanks were spiked with 1.5 mg ^{27}Al carrier (Fischer Al carrier, 1000 ppm) and samples were spiked with up to 1.5 mg ^{27}Al carrier (the latter value varied depending on the native Al-content of the sample). Blanks range from $5 \times 10^{-15} - 3 \times 10^{-14}$ [^{10}Be/^{9}Be] (less than 5% of total ^{10}Be atoms in all but the youngest samples); and $2 \times 10^{-15} - 2 \times 10^{-14}$ [^{26}Al/^{27}Al] (less than 2% of total ^{26}Al atoms in all but the youngest samples). Concentrations in Table 1 are corrected for process blanks; uncertainties include propagated AMS sample/lab-blank uncertainty, a 2% carrier mass uncertainty, and a 3% stable ^{27}Al measurement (ICP-OES) uncertainty.

2.3. Exposure age calculations

For exposure age calculations we used default settings in Version 2.0 of the CRONUScalc programme (Marrero et al., 2015). The CRONUS-Earth production rates (Borchers et al., 2015) with the nuclide-dependent scaling of Lifton-Sato-Dunai (Lifton et al., 2014) were used to calculate the ages presented in the paper. Sea level and high latitude production rates are 3.92 ± 0.31 atoms $g^{-1}a^{-1}$ for ^{10}Be and 28.5 ± 3.1 atoms $g^{-1}a^{-1}$ for ^{26}Al. The alternative use of Lal/Stone (Lal, 1991; Stone, 2000) scaling does not change the conclusions of the paper despite the approximately 3% and 6% older exposure ages for ^{10}Be and ^{26}Al, respectively. Rock density is assumed 2.7 g cm^{-3} and the attenuation length used is 153 ± 10 g cm^{-2}. No corrections are made for rock surface erosion or snow cover and thus exposure ages are minima. Finally, we make no attempt to account for the relatively minor production-rate variations that would be caused by elevation changes associated with glacial isostatic adjustment of the massif through time (Stone, 2000; Suganuma et al., 2014). All ages are apparent exposure ages, which make the assumptions that all exposure has been achieved in a single episode at the current location of the sample, that the sample has not been covered by snow or sediment, and has experienced zero erosion.

3. Results

From the sediments, moraines and erosional landforms preserved in the Neptune and Patuxent Ranges we have identified

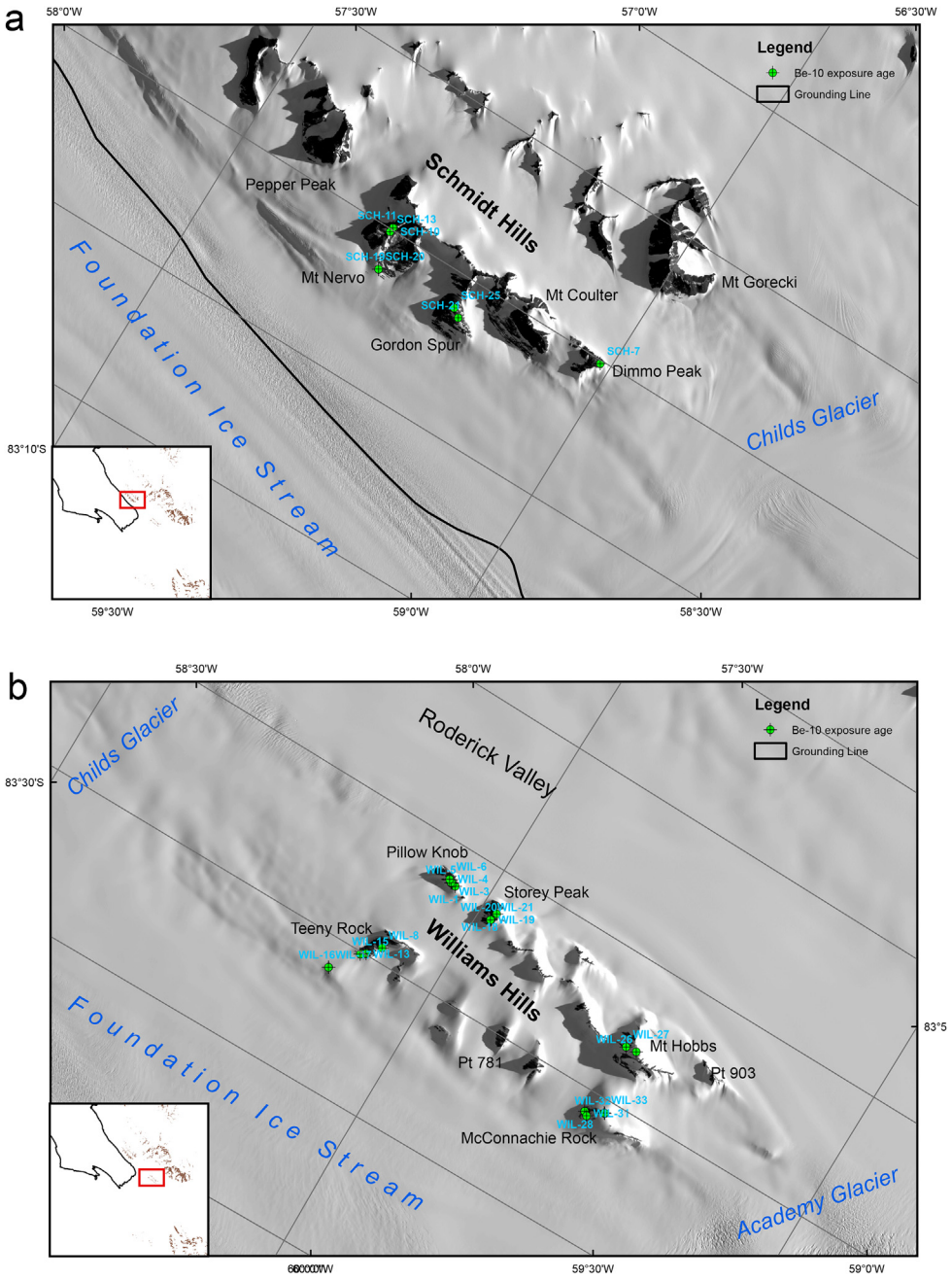

Fig. 2. Field sites and sample locations. (a) Schmidt Hills, (b) Williams Hills, (c) Mt Bragg and Mt Harper, (d) Thomas Hills. Background imagery in a and b is USGS Landsat 8 satellite imagery (Band 8). Background maps in c and d are the USGS 1:250,000 Reconnaissance Series Topographic Maps of Antarctica (Sheets: SU21-25/13 (Schmidt Hills), SV21-30/1 (Gambacorta Peak) and SV11-20/4 (Thomas Hills). Place names proposed and adopted by the UK Committee on Antarctic Place Names have been added. Cosmogenic nuclide sample locations are shown as green dots. See Tables 1 and 2 for sample data. (For interpretation of the references to colour in this figure legend, the reader is referred to the web version of this article.)

evidence for ice sheet expansion (thickening) and retreat (thinning). The area shows abundant evidence of thicker ice, with sandstone erratics strewn over most surfaces visited (Fig. 3a). A small number of features provide evidence of former ice limits (e.g., Fig. 3b), and in some cases show complex and repeated interaction of different ice masses (Fig. 3c). In all cases we sampled erratics over altitudinal profiles from the summits to the present ice margin. The exposure ages of these erratics yields a thinning history for the Foundation Ice Stream and Academy Glacier, which is presented after a description of the glacial geomorphology of the sample sites.

3.1. Geomorphology

The erratic lithologies in the Neptune Range are dominated by Dover Sandstone (white to yellow, medium to coarse-grained, finely bedded to massive, quartz-rich) (Schmidt et al., 1978). Erratics are found on at least the lower parts of almost every nunatak visited, and in many cases are abundant. There are fewer Dover Sandstone erratics on nunataks in the Patuxent Range: here erratic lithologies tended to be darker-coloured, harder and finer-grained sandstones. Although not generally sampled, other erratic lithologies seen on nunataks include sandstone with conglomeratic

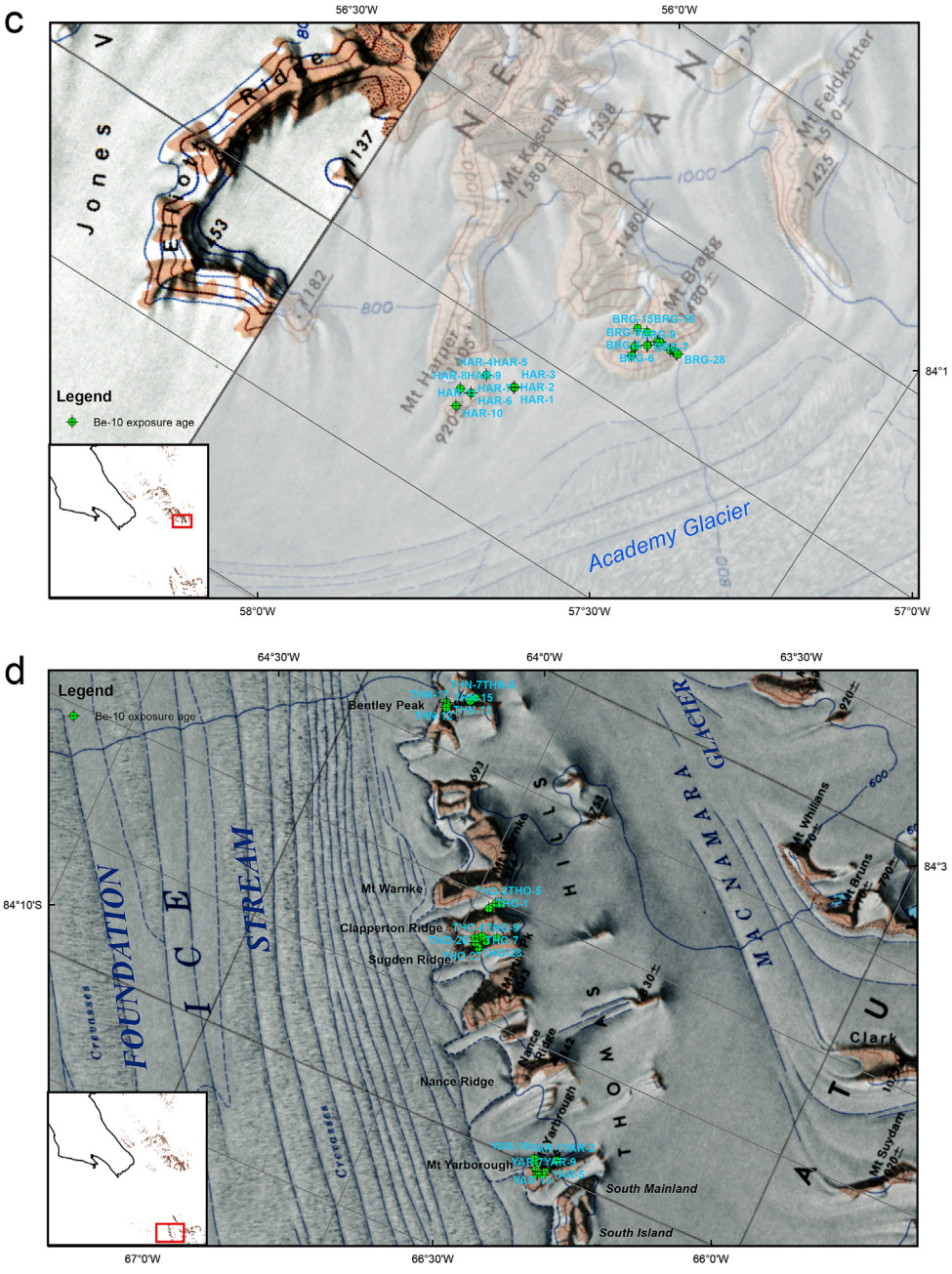

Fig. 2. (*continued*).

layers (including granodiorite pebbles), basalt (fine-grained, weathered, rounded, ventifacted), dolerite-gabbro (coarse, angular blocks), granodiorite (pebble and small cobbles only), granite, gneiss and limestone. Some sandstone erratics show one or more of granular disaggregation, spalling and tafoni. Whilst overall across the study area the erratics are of diverse lithologies, we focused sampling on the Dover Sandstone clasts as they were the commonest clasts at most localities and had a fresher appearance than some of the basalt (ventifacted) or other sandstone (tafoni weathering) clasts. A few Dover Sandstone clasts had a darker yellow weathered outer surface; these were avoided in sampling.

Many of the slopes in the area are mantled by a veneer of debris, much of it made up of a layer (>30 cm thick) of pale yellow-brown (fresh) to khaki brown (weathered) silty diamict, with locally-derived clasts, and open pore spaces up to a few mm across. The diamict has a hard crust and is also partially-cemented. Surface salt encrustation of this diamict is common. Some slopes have small terraces, 2–4 m across with risers of 30–50 cm. Exposures of the diamict are common in these risers or in frost cracks that cut through the terracing. Such features are particularly common downslope of snow patches, probably due to availability of liquid water. This diamict underlies talus slopes, desert pavement cover and many of the erratics sampled by us, but it is not ubiquitous and some of the nunataks, especially in the Schmidt Hills and parts of the Thomas Hills, do not have exposures of a diamict. In these locations there is a felsenmeer of locally-derived bedrock on low-angle slopes.

Many nunataks have areas of striated bedrock. For example, in Williams Hills, the bedrock on Pillow Knob (NE end) is well-striated with two generations of striations. The first is finely-spaced, mm-

Table 1
Rock sample details and cosmogenic ^{10}Be and ^{26}Al concentrations in quartz-bearing erratics.

Location	Sample ID	Lat. (dd)	Long. (dd)	Alt. (m asl)	Lithology[a]	Thickness (cm)	Topo shielding	Quartz mass (g)	^{10}Be AMS ID[b]	^{10}Be concn[c] (atom g^{-1}[SiO$_2$])	±1σ ^{10}Be (atom g^{-1} [SiO$_2$])	^{26}Al AMS ID[b]	^{26}Al concn[d] (atom g^{-1}[SiO$_2$])	± 1σ ^{26}Al atom g^{-1} [SiO$_2$])
Pillow Knob	WIL-1	−83.65392	−58.63597	689	Qtz ss	3.0	0.999	30.933	b4558	6.536E+04	3.219E+03			
Pillow Knob	WIL-3	−83.65240	−58.63180	722	P congl.	3.5	0.997	29.819	b4559	6.007E+04	2.679E+03			
Pillow Knob	WIL-4	−83.65185	−58.63303	743	Qtz ss	4.0	0.998	26.054	b7805	5.180E+04	4.176E+03			
Pillow Knob	WIL-5	−83.65182	−58.63197	746	Qtz ss	4.0	0.998	28.863	b5258	8.226E+04	2.785E+03	a2004	5.228E+05	3.620E+04
Pillow Knob	WIL-6	−83.65067	−58.62528	780	P congl.	4.0	1.000	28.513	b7806	7.512E+04	5.347E+03			
Teeny Rock	WIL-8	−83.64213	−58.95122	572	Qtz ss	4.5	0.999	29.004	b4564	5.440E+04	2.792E+03			
Teeny Rock	WIL-13	−83.63807	−58.99585	529	Qtz ss	3.5	1.000	32.214	b5259	4.762E+04	2.038E+03	a2005	3.178E+05	2.389E+04
Teeny Rock	WIL-15	−83.63615	−59.00812	500	Qtz ss	3.5	1.000	31.494	b4565	5.794E+04	3.458E+03			
Teeny Rock	WIL-16	−83.62843	−59.10403	459	Qtz ss	4.5	1.000	26.893	b5260	2.604E+06	7.854E+04			
Teeny Rock	WIL-17	−83.62835	−59.10415	442	Qtz ss	3.0	1.000	26.474	b4566	4.085E+04	2.701E+03			
Storey Peak	WIL-18	−83.67310	−58.64347	861	Qtz ss banded	4.0	1.000	27.880	b5261	1.214E+05	4.375E+03			
Storey Peak	WIL-19	−83.67243	−58.66825	841	Qtz phenocryst	6.0	1.000	24.468	b7807	7.137E+04	4.185E+03			
Storey Peak	WIL-20	−83.67233	−58.67065	838	Qtz ss	5.0	1.000	27.784	b5262	9.142E+04	3.785E+03			
Storey Peak	WIL-21	−83.67223	−58.67187	831	SS impure	8.0	1.000	28.355	b4568	1.059E+05	4.977E+03			
Mt Hobbs	WIL-26	−83.74648	−58.80223	1055	Qtz ss	4.0	1.000	25.519	b4569	1.217E+05	5.115E+03			
Mt Hobbs	WIL-27	−83.74212	−58.80662	1055	Qtz microcrystalline	3.0	1.000	4.565	b5264	6.866E+06	2.131E+05			
McConnachie Rock	WIL-28	−83.74122	−59.07610	621	Qtz ss	3.5	0.998	28.801	b4570	5.396E+04	3.079E+03			
McConnachie Rock	WIL-31	−83.74275	−59.08593	665	Qtz ss fine/grey	3.5	0.999	26.641	b7809	1.043E+06	2.879E+04			
McConnachie Rock	WIL-32	−83.74827	−59.04553	796	Qtz ss	3.5	1.000	28.008	b4574	8.821E+04	3.818E+03			
McConnachie Rock	WIL-33	−83.74803	−59.04458	795	Qtz ss	5.0	1.000	29.350	b7810	7.489E+04	3.831E+03			
Mt Bragg	BRG-1	−84.09852	−56.78165	1048	Qtz ss	3.0	0.999	26.368	b4575	2.686E+05	7.721E+03			
Mt Bragg	BRG-2	−84.09852	−56.78250	1047	Qtz ss	6.0	0.999	27.818	b7816	1.862E+05	5.954E+03			
Mt Bragg	BRG-4	−84.09835	−56.78345	1049	Qtz ss banded	3.5	0.999	32.423	b7817	1.087E+05	3.788E+03			
Mt Bragg	BRG-5	−84.09655	−56.80657	1002	Qtz ss pebble	3.5	0.997	28.681	b4576	2.559E+06	5.768E+04			
Mt Bragg	BRG-6	−84.09652	−56.80710	1000	Qtzite banded	4.0	0.997	25.686	b5266	5.306E+05	1.677E+04			
Mt Bragg	BRG-7	−84.09652	−56.80768	1000	Qtz ss	3.0	0.997	29.849	b5267	9.543E+05	3.007E+04			
Mt Bragg	BRG-8	−84.09650	−56.80785	1000	Qtz ss	5.5	0.997	27.404	b4577	4.660E+05	1.236E+04			
Mt Bragg	BRG-9	−84.09373	−56.83290	898	Qtz ss	3.5	0.990	29.200	b7818	1.661E+06	4.394E+04			
Mt Bragg	BRG-10	−84.09368	−56.82920	900	Qtz ss	6.0	0.990	26.916	b7819	1.775E+06	4.009E+04			
Mt Bragg	BRG-11	−84.09430	−56.85667	814	Qtz ss red/banded	5.0	0.994	26.708	b4579	1.497E+06	3.346E+04			
Mt Bragg	BRG-13	−84.09142	−56.78210	1196	Qtz ss	5.0	1.000	25.928	b4580	4.977E+06	1.091E+05			
Mt Bragg	BRG-14	−84.09138	−56.78278	1196	Qtz ss	4.0	1.000	29.499	b7820	2.730E+05	8.882E+03			
Mt Bragg	BRG-15	−84.09433	−56.77607	1125	Qtz ss	4.0	0.999	30.048	b4581	2.057E+06	4.622E+04			
Mt Bragg	BRG-16	−84.09433	−56.77607	1125	Qtz ss	3.0	0.999	28.414	b7822	5.259E+06	1.096E+05			
Mt Bragg	BRG-19	−84.09908	−56.77937	1030	Qtz ss	3.0	0.996	30.337	b4590	2.078E+06	4.578E+04			
Mt Bragg	BRG-20	−84.09907	−56.78190	1030	Qtz ss	3.0	0.996	28.145	b5270	1.591E+05	5.159E+03	a2007	1.113E+06	6.579E+04
Mt Bragg	BRG-21	−84.10288	−56.78340	920	Qtz ss	5.5	0.994	26.161	b4591	1.712E+06	3.831E+04			
Mt Bragg	BRG-22	−84.10285	−56.78333	920	Qtz ss	6.0	0.994	26.563	b5271	1.568E+06	4.741E+04			
Mt Bragg	BRG-23	−84.10428	−56.77825	870	Qtz ss	3.0	0.994	27.583	b4592	3.105E+06	6.851E+04			
Mt Bragg	BRG-24	−84.10417	−56.77890	872	Qtz ss	7.0	0.994	25.963	b5272	1.255E+06	3.874E+04			
Mt Bragg	BRG-25	−84.10485	−56.78243	842	Qtz ss grey	3.5	0.992	26.301	b4593	2.245E+06	4.949E+04			
Mt Bragg	BRG-26	−84.10495	−56.78202	840	Qtz ss	3.5	0.992	32.044	b5273	4.620E+04	2.148E+03	a2008	3.076E+05	2.604E+04
Mt Bragg	BRG-27	−84.10540	−56.78197	816	Qtz ss	5.0	0.898	29.210	b4595	2.536E+04	1.788E+03			
Mt Bragg	BRG-28	−84.10537	−56.78232	813	Qtz ss	3.5	0.898	32.358	b5274	2.338E+05	7.478E+03			
Mt Harper	HAR-1	−84.07052	−57.11272	878	Qtz ss	3.5	1.000	29.411	b5277	5.215E+04	2.193E+03	a2011	3.943E+05	2.978E+04
Mt Harper	HAR-2	−84.07055	−57.11340	878	Qtz ss	4.5	1.000	31.937	b5278	4.940E+04	1.988E+03			
Mt Harper	HAR-3	−84.07080	−57.11153	878	Qtz ss	4.0	1.000	28.348	b7811	3.738E+04	3.079E+03			
Mt Harper	HAR-4	−84.06193	−57.12530	913	Qtz ss	4.0	1.000	24.055	b4827	7.461E+04	3.089E+03			
Mt Harper	HAR-5	−84.06193	−57.12530	913	Qtz ss	4.0	1.000	27.739	b5279	6.918E+04	2.568E+03	a2012	5.346E+05	3.718E+04
Mt Harper	HAR-6	−84.06105	−57.19130	840	Qtz ss	3.5	1.000	31.845	b4596	7.855E+04	3.565E+03			
Mt Harper	HAR-7	−84.06100	−57.19182	840	Qtz ss	3.5	1.000	28.209	b5282	8.732E+04	3.181E+03	a2013	6.521E+05	4.638E+04
Mt Harper	HAR-8	−84.05772	−57.19725	782	Qtz ss	6.0	0.999	28.401	b5283	5.514E+04	2.260E+03			
Mt Harper	HAR-9	−84.05772	−57.19725	780	Qtz ss banded	4.5	0.999	28.276	b5284	3.608E+05	1.151E+04			
Mt Harper	HAR-10	−84.05935	−57.24463	734	Qtz ss	2.5	0.999	29.241	b4597	1.544E+05	5.735E+03			
Mt Harper	HAR-11	−84.05935	−57.24463	734	Qtz ss	7.0	0.999	30.887	b5285	9.731E+04	3.614E+03			

(*continued on next page*)

Table 1 (*continued*)

Location	Sample ID	Lat. (dd)	Long. (dd)	Alt. (m asl)	Lithology[a]	Thickness (cm)	Topo shielding	Quartz mass (g)	^{10}Be AMS ID[b]	^{10}Be concn[c] (atom g^{-1}[SiO$_2$])	±1σ ^{10}Be (atom g^{-1} [SiO$_2$])	^{26}Al AMS ID[b]	^{26}Al concn[d] (atom g^{-1}[SiO$_2$])	± 1σ ^{26}Al atom g^{-1} [SiO$_2$])
Dimmo Peak	SCH-7	−83.32930	−58.01092	560	Qtz ss	6.0	0.993	25.140	b5246	1.891E+06	5.726E+04			
Mt Nervo	SCH-10	−83.23432	−57.99215	874	Qtz ss	2.5	1.000	27.294	b5247	1.292E+07	2.851E+05			
Mt Nervo	SCH-11	−83.23410	−57.99407	876	Qtz pegmatite	5.5	1.000	26.899	b5248	1.796E+07	3.809E+05			
Mt Nervo	SCH-13	−83.23402	−58.00913	829	Qtz ss	3.5	0.998	30.311	b5249	6.426E+06	1.422E+05			
Mt Nervo	SCH-19	−83.23785	−58.13295	400	Qtz ss	3.5	0.999	30.525	b5250	2.139E+06	6.429E+04			
Mt Nervo	SCH-20	−83.23780	−58.13248	401	Qtz ss banded	5.0	0.999	26.490	b5252	1.993E+06	5.724E+04			
Gordon Spur	SCH-21	−83.27373	−58.13032	667	Qtz	5.0	1.000	29.030	b5253	1.032E+07	2.269E+05			
Gordon Spur	SCH-25	−83.27035	−58.10953	728	Qtz ss banded	5.0	1.000	28.297	b5255	8.647E+06	1.907E+05			
Clapperton Ridge	THO-1	−84.34060	−65.04507	730	Qtz ss banded	5.0	1.000	31.741	b4804	7.129E+06	1.594E+05			
Clapperton Ridge	THO-3	−84.34245	−65.01345	782	Qtz ss	4.5	0.998	26.591	b4807	7.128E+06	1.534E+05	a1406	3.382E+07	1.742E+06
Clapperton Ridge	THO-5	−84.34458	−65.00268	840	Qtz	5.0	0.998	30.046	b4808	8.510E+06	1.899E+05	a1409	3.983E+07	2.037E+06
Sugden Ridge	THO-7	−84.34243	−65.19182	465	Qtz ss fine	5.0	0.986	27.083	b4809	3.120E+05	1.013E+04			
Sugden Ridge	THO-8	−84.34248	−65.19147	465	Qtz ss	4.0	0.986	30.234	b4810	1.947E+05	6.561E+03			
Sugden Ridge	THO-9	−84.34248	−65.19147	465	Qtzite	4.0	0.986	26.553	b6690	2.263E+05	7.773E+03	a2017	1.570E+06	9.190E+04
Sugden Ridge	THO-10	−84.34248	−65.19147	465	Qtz ss grey	6.0	0.986	27.895	b6691	2.208E+05	8.796E+03	a2018	1.371E+06	8.391E+04
Sugden Ridge	THO-11	−84.34565	−65.18108	520	P. congl.	5.0	0.988	25.974	b4811	4.131E+05	1.212E+04			
Sugden Ridge	THO-12	−84.34560	−65.18220	530	Qtz ss fine	3.0	0.988	32.211	b4813	2.732E+05	7.576E+03			
Sugden Ridge	THO-13	−84.34315	−65.16932	414	Qtz ss	4.5	0.993	26.538	b4815	2.633E+05	8.573E+03			
Sugden Ridge	THO-14	−84.34313	−65.16890	414	Qtz ss	3.0	0.993	28.066	b4816	2.110E+05	6.868E+03			
Sugden Ridge	THO-15	−84.34310	−65.16948	414	Qtz ss grey	3.5	0.993	25.286	b6693	9.605E+04	4.508E+03	a2019	6.546E+05	4.278E+04
Sugden Ridge	THO-16	−84.34312	−65.16980	414	Qtz ss fine	3.0	0.993	25.511	b6694	1.744E+05	6.502E+03	a2020	1.133E+06	6.609E+04
Sugden Ridge	THO-17	−84.34065	−65.18838	410	Qtz ss	4.0	0.992	27.548	b4819	3.376E+05	1.055E+04			
Sugden Ridge	THO-18	−84.34063	−65.18847	410	Qtz ss	3.0	0.992	26.848	b4820	2.152E+05	6.114E+03			
Sugden Ridge	THO-19	−84.34055	−65.18920	410	Qtz ss	4.0	0.992	26.434	b6695	2.587E+06	6.105E+04			
Sugden Ridge	THO-20	−84.34055	−65.18918	410	Qtz ss	4.0	0.992	29.049	b6696	2.147E+06	5.123E+04			
Sugden Ridge	THO-21	−84.34915	−65.14835	545	Qtz	4.0	0.998	29.180	b4821	4.187E+06	9.144E+04	a1411	2.318E+07	1.213E+06
Sugden Ridge	THO-24	−84.34355	−65.22095	635	Qtz ss	5.0	0.999	30.388	b4822	8.690E+05	2.201E+04	a1412	5.858E+06	3.152E+05
Sugden Ridge	THO-25	−84.34150	−65.20867	480	Qtz ss	3.5	0.970	28.501	b6697	1.309E+06	3.463E+04			
Sugden Ridge	THO-26	−84.34152	−65.20773	477	Qtzite green	3.5	0.970	26.327	b6702	1.405E+06	3.799E+04			
Sugden Ridge	THO-27	−84.34155	−65.20773	477	Qtz ss pebbles	5.0	0.984	29.669	b4823	2.313E+05	7.590E+03			
Sugden Ridge	THO-28	−84.34155	−65.20689	475	Qtz ss pebbles	4.0	0.984	25.036	b4826	2.650E+05	9.416E+03			
Bentley Peak	THN-7	−84.29638	−64.23857	570	Qtz ss	3.5	0.998	29.953	b6709	4.196E+06	9.372E+04			
Bentley Peak	THN-8	−84.29648	−64.23945	570	Qtz pegmatite	3.0	0.998	30.031	b6711	4.586E+06	1.033E+05			
Bentley Peak	THN-10	−84.29493	−64.26187	515	Qtz ss fine	4.0	0.999	29.965	b6715	3.801E+04	5.815E+03	a2023	3.337E+05	2.404E+04
Bentley Peak	THN-12	−84.28612	−64.31283	390	Qtz ss coarse	3.5	0.998	27.224	b6716	3.751E+05	1.453E+04			
Bentley Peak	THN-13	−84.28595	−64.31307	390	Qtz ss fine	3.5	0.998	25.248	b6717	5.929E+05	2.558E+04			
Bentley Peak	THN-15	−84.28683	−64.32338	435	Qtz ss	4.0	0.998	28.907	b6718	5.490E+05	2.015E+04			
Bentley Peak	THN-17	−84.28683	−64.33273	463	Qtzite	3.5	0.997	27.667	b6719	3.588E+05	1.398E+04			
Mt Yarborough	YAR-1	−84.41220	−65.93483	848	Qtz ss fine	4.5	0.999	26.235	b4837	7.647E+06	1.668E+05	a1421	3.711E+07	1.887E+06
Mt Yarborough	YAR-2	−84.41225	−65.93440	850	Qtz ss	5.5	0.999	27.533	b4838	8.145E+06	1.820E+05			
Mt Yarborough	YAR-5	−84.41005	−65.99980	790	Qtz ss fine	6.0	1.000	32.110	b4839	5.143E+06	1.126E+05	a1422	2.975E+07	1.516E+06
Mt Yarborough	YAR-7	−84.40942	−66.01725	768	Qtz ss	4.0	0.999	29.899	b4840	6.424E+06	1.437E+05			
Mt Yarborough	YAR-9	−84.40735	−66.02582	710	Qtz ss	6.0	0.999	31.709	b4843	3.286E+06	7.102E+04			
Mt Yarborough	YAR-11	−84.40703	−66.01277	690	Qtz ss	4.5	0.998	24.883	b4844	2.341E+06	5.337E+04			
Mt Yarborough	YAR-12	−84.40700	−66.01237	690	Qtz ss	5.0	0.998	26.325	b6703	3.266E+06	7.319E+04			
Mt Yarborough	YAR-14	−84.40555	−65.99897	670	Qtz ss	3.0	0.998	31.048	b6704	5.258E+06	1.139E+05			
Mt Yarborough	YAR-15	−84.40395	−65.97610	642	Qtz ss pink	5.0	0.998	29.025	b6705	3.038E+06	6.669E+04			
Mt Yarborough	YAR-16	−84.40403	−65.97715	644	Qtz ss	4.0	0.998	26.872	b4845	4.426E+06	9.967E+04			
Mt Yarborough	YAR-17	−84.40345	−65.96642	615	Qtz pegmatite	7.0	0.993	30.595	b6707	4.396E+06	9.391E+04			
Mt Yarborough	YAR-18	−84.40342	−65.96640	615	Qtz ss	4.0	0.993	29.136	b6708	5.360E+06	1.143E+05			

[a] SS: sandstone; Qtz: quartz; Qtzite: quartzite; P. congl.: pebble conglomerate. Assumed rock density 2.7 g cm^{-3}.

[b] AMS measurements made at Scottish Universities Environmental Research Centre (SUERC).

[c] Normalised to NIST SRM-4325 Be standard material with a revised nominal ^{10}Be/^{9}Be ratio (2.79×10^{-11}) (Nishiizumi et al., 2007) and corrected for process blanks; uncertainties include propagated AMS sample/lab-blank uncertainty and a 2% carrier mass uncertainty.

[d] Normalised to the Purdue Z92-0222 Al standard material with a nominal ^{27}Al/^{26}Al ratio of 4.11×10^{-11} that agrees with Al standard material of Nishiizumi, (2004), and corrected for process blanks; uncertainties include propagated AMS sample/lab-blank uncertainty and a 5% stable ^{27}Al measurement (ICP-OES) uncertainty.

scale, regular and extends across bedrock surfaces for 10s of cm (Fig. 3d). These have a distinct weathering sheen or patina over the surface. Their trend is 050–230°. These striations are found commonly on surfaces all over the upper ridge and on the summit. The second, cross-cutting set of striations are irregular, cm-scale 'gouges' (up to 1 cm wide, but usually 2–5 mm wide) that cut into the weathering patina, and are oriented approximately 100–280°. They incise (1–2 mm) the patina and are themselves not weathered (Fig. 3d). These gouges are not continuous (unlike the earlier striation set) and can be identified as individual gouges up to 12–15 cm long, but usually only up to 5 cm. We follow Atkins et al. (2002) and Bentley et al. (2006) in interpreting the two sets of striations as evidence for an early warm-based ice sheet (closely-spaced, polished, weathered striations) followed by a later cold-based ice sheet (unweathered, less regular gouges). However, at one location on the NE side of Pillow Knob both sets appear more closely-spaced, regular and equally weathered, and so we cannot rule out that the second ice sheet was warm-based, at least in parts.

Bedrock throughout the area is usually weathered with a dark red surface patina. Locally-derived talus is common on steeper slopes and in places this overlies either the bedrock or the silty diamict. Both the weathered bedrock and the silty diamict extend right down to the present ice surface.

3.1.1. Schmidt Hills

The Schmidt Hills are a line of nunataks along the east side of the Foundation Ice Stream, close to its grounding line (Fig. 2a). Spurs from these nunataks extend west down to the ice margin, at ~200–300 m asl. Erratics are rare on all nunataks in the Schmidt Hills. For example on Dimmo Peak, only two true erratics (one sandstone, one granitic) were found in the 400 m elevational range between the ice edge on the SE side of the nunatak and the summit, and both were found at a relatively low elevation. At ~860 m on the W ridge of Mt. Nervo there is a local concentration of sandstone and conglomerate erratics that are of sufficient lithological and colour/weathering diversity for us to be confident that they are not originally derived from a single clast.

No striations were found on summits and virtually all the bedrock surfaces have weathered surfaces (Fig. 3e). Lower down (below ~ 600 m asl) there are many striated surfaces on a spur W of Dimmo Peak, with trend 036–216 to 056–236°. Lower parts of the spurs in Schmidt Hills also appear more rounded than the summits. Diamict occurs over parts of the nunataks but is more commonly exposed on the lower spurs, where the debris cover is modified by surficial mass movement. In several locations on the S side of Mt. Nervo (e.g., 83° 14.494 S, 057° 56.440 W, 975 m) there are bedrock fractures that have been filled by diamict.

The degree of weathering increases upwards on Mt. Nervo and Mt. Coulter such that near the summits there are features such as tafoni weathering, spalling, and thick weathering rinds. The ridge crests themselves are weathered such that cleaved sedimentary bedrock forms soft friable surfaces, whilst basalts have weathered into nodules. Bowl-shaped depressions a few 100 m across on the flanks of these nunataks contain extensive periglaciated (polygons, stripes, terraces, deep frost cracks) deposits containing pale yellow silty diamict, >30 cm thick. At the mouth of the bowl on the SW flank of Mt. Nervo there are prominent morainic deposits forming a mantle of debris over linear bedrock features sub-parallel to the Foundation Ice Stream margin.

3.1.2. Williams Hills

The Williams Hills have abundant erratics at all elevations, lying on the yellow silty diamict, on felsenmeer, on summit plateaux, or on bedrock (Fig. 2b). The vast majority of these are erratics of Dover sandstone. There is also evidence of ice transport of local lithologies (translocation of clasts from host outcrops on flat surfaces or uphill). Weathered, pervasively striated bedrock shows 'old' overriding (warm-based) glaciations trending 035–215° (Mt. Hobbs) or 050–230° (Pillow Knob). Fresher striations trend 100–280° and are scattered and more gouge-like (cold-based). The yellow diamict is ubiquitous over all surfaces, from the modern ice edge to the highest summit (Mt. Hobbs).

3.1.3. Mt. Harper and Mt. Bragg

Along the northern margin of the Academy Glacier there are a series of nunataks that have a geological record of glacier fluctuations on their southern flanks. The westernmost of these is Mt. Harper, with Mt. Bragg to the east (Fig. 2c). There are extensive blue ice areas with supraglacial moraines along this margin of the Academy Glacier.

Mt. Harper has a series of low knolls directly south of the main nunatak. These are mantled in a veneer of drift that is composed mainly of the local basaltic lithology but with abundant freshly weathered sandstone clasts. There is an underlying sandy diamict present but this is generally confined to pockets in bedrock.

The most prominent glacial feature on Mt. Bragg is a distinctive line of boulders located about 200 m above the present ice surface and which can be traced wrapping continuously around the slopes of Mt. Bragg for up to 2 km (Fig. 3b). The boulder moraine is composed of off-white to yellow erratics. To the east (up-ice) it cannot be traced beyond a talus slope directly below the summit of Mt. Bragg. To the west (down-ice) the limit descends parallel to the modern glacier margin below. There is no apparent difference in weathering of bedrock on either side of the boulder limit, and a small number of fresh sandstone erratics are found on the slopes immediately above it. Bedrock on Mt. Bragg has a reddish-brown to purple weathering sheen, and in places has polish and striations. The striations are mm-scale, finely-spaced, trend 077–257° and are widely distributed.

Higher up, the west summit (1200 m) of Mt. Bragg is highly weathered with an orange-brown patina and ubiquitous frost-shattering of bedrock. The number of erratics mantling the surface is much less than lower on the nunatak, and the erratics themselves are more weathered than those lower down. In particular volcanic erratic clasts have polish, weathering patina and ventifaction.

On the south side of the Academy Glacier we sampled former lake shorelines in the Mt. Lowry region: these may record ice sheet thinning (see Hodgson and Bentley (2013) for full description). The lake shorelines are covered by sub-fossil microbial mats that have desiccated into grey papery deposits that are found preserved under cobbles and boulders.

3.1.4. Thomas Hills

The Thomas Hills comprise a series of NW-SE trending ridges that flank the east side of the Foundation Ice Stream, upstream of its confluence with the Academy Glacier (Fig. 2d). Here we report the geomorphology from the spurs[1] of Mt. Yarborough, Sugden Ridge, Clapperton Ridge, and Bentley Peak.

3.2. Mt. Yarborough

Mt. Yarborough sits towards the SW end of the Thomas Hills. Most of the nunatak is mantled in morainic debris and numerous erratics. Striations near the summit of Mt. Yarborough and close to

[1] Only a few of the spurs in the Thomas Hills are named on the 1960s USGS map and so in 2011 the UK Antarctic Place Names Committee named the previously unnamed spurs.

the ice margin trend 119–299°, and lower slopes are mantled in a silty white diamict. Erratics are numerous and were sampled from the summit down to the edge of the Foundation Ice Stream.

3.3. Sugden Ridge

The glacial geomorphology preserved on this ridge records the interaction between the Foundation Ice Stream and more locally-sourced ice spilling over from the MacNamara Glacier to the south-east. The Foundation Ice Stream is higher than the area between the spurs of the Thomas Hills and so lobes of the Foundation Ice Stream flow downhill into the embayments, each of them terminating in an area of blue-ice, and hence net ablation. At the northern end of the ridge there is a small lobe of Foundation Ice Stream ice that flows down to the SE into the valley between Sugden and Clapperton Ridges, and former positions of this lobe are marked by a series of lateral moraines on the NE flank of Sugden Ridge. Each of these moraines consists of distinct lines of pale sandstone boulders, except for the lowest moraine close to the present Foundation Ice Stream margin, which constitutes a substantial ridge of diamict a few metres high. The moraines range in elevation from just a few metres above the present ice margin (370 m asl) to 150 m above the present ice, and have gradients consistent with formerly expanded Foundation Ice Stream ice. Similarly, former positions of a lobe derived from the MacNamara Glacier that spilled over the col between the two ridges and flowed NW towards the Foundation Ice Stream are also recorded on the same slope. Some of these moraine sequences intersect and overlap (Fig. 3c). Finally there is an area of patterned ground – probably representing former snowpatches – that descends NE-wards from the middle of the ridge forming Sugden Ridge (Fig. 3c). The northern ridge summit above the moraines is striated whilst the southern parts of the ridge are mantled in silty diamict with a widespread surface salt encrustation.

3.4. Clapperton Ridge

The sandstone bedrock of Clapperton Ridge is deeply weathered, striated in places and an overlying silty diamict is widespread, including overlying striated bedrock. Striations in a col on the ridge trend 129–309°, and are of the extensive, finely-spaced (warm-based) type. No scattered striations or gouges (cold-based) were seen cutting them.

3.5. Bentley Peak

This minor peak lies at the NE end of Thomas Hills. Striae are visible at all altitudes on this nunatak, and trend 130–310°. We sampled a transect of erratics and quartz bedrock veins from the summit (715 m) down to the Foundation Ice Stream margin at 490 m. The lowest part of the nunatak is mantled in a thick diamict that has an unweathered appearance and contains fresh, unweathered erratics.

3.5.1. Geomorphological interpretation

There is a consistent pattern of glacial geomorphology in the Pensacola Mountains. Specifically there is evidence of at least two major glacial phases or configurations: the first of these was a warm-based glaciation that striated bedrock across the field area and flowed oblique to present-day ice flow. For example, in the Williams Hills, modern ice flow is northwards, but striations show former flow aligned NE-SW. This may have been the same glacial phase that deposited a near-ubiquitous silty yellow diamict across the field area and which occurs directly over many of the striated surfaces. The weathering of the striated surfaces and of the diamict itself suggests that this glaciation was old, and we cannot rule out that the diamict is an equivalent of the Sirius Group diamictons or other several-million year old diamicts found elsewhere in the Transantarctic Mountains. A second glacial phase constituted a cold-based ice sheet expansion that over-rode and striated several summits, for example, in the Williams Hills. There is little other evidence of erosion, and ice flowed obliquely to the earlier phase. This second phase is associated with the deposition of erratics across almost all surfaces, as well as a fresh diamict in a few places. Thinning from this glaciation left boulder moraines recording former ice margins along the side of Mt. Bragg and Thomas Hills, and erratics located from summits to present ice elevations. During this period, there were interactions between an expanded Foundation Ice Stream/Academy Glacier and more locally-sourced ice, such as is recorded in the Thomas Hills.

The Schmidt Hills are anomalous in this regional pattern in that they contain few erratics. Where they do occur they tend to cluster in highly localized concentrations, such as on the W ridge of Mt. Nervo. In the Schmidt Hills and in some of the Thomas Hills there is a consistent pattern of summits being significantly more weathered than lower reaches.

3.5.2. Cosmogenic nuclide exposure ages

We sampled and analysed 105 erratics to derive their exposure ages using cosmogenic nuclides. The exposure ages ranged from 2.5 ka to 3 Ma but with significant clustering of ages <10 ka. When plotted against their height above present day ice the younger ages in two of the four areas studied show clear thinning trajectories in the Holocene (Table 2, Fig. 4): Williams Hills and the closely adjacent sites of Mt. Bragg and Mt. Harper. Other sites show more complex histories of ice sheet fluctuations (Fig. 4). In all four areas the analysed samples include a component of older material, a common feature of cosmogenic isotope-derived chronologies of ice sheet thinning in Antarctica (Balco, 2011; Balco et al., 2016; Bentley et al., 2006, 2010; Hein et al., 2011, 2014; Mackintosh et al., 2011) caused by individual clasts being recycled or overridden during ice sheet thickening-thinning cycles. In the case of the subset of older samples analysed for ^{26}Al these all yielded discordant ages implying a complex exposure history with at least one period of burial.

3.5.2.1. Schmidt Hills. In the Schmidt Hills, of the eight erratic samples analysed, there are no samples younger than 236 ka, and most are substantially older, up to 3 Ma (Fig. 4a). Whilst there may be a partial record of fluctuations over successive glacial cycles the site does not provide any constraints on deglaciation from the LLGM.

3.5.2.2. Williams Hills. Of the 20 cosmogenic exposure dates 17 yield Holocene ages and show that thinning of the ice sheet occurred from at least 450 m above present ice elevations. This thinning was progressive from the Early to mid-Holocene and reached 50 m above present-day ice by 5 ka. Notably there are no samples younger than 5 ka (Fig. 4b and c).

3.5.2.3. Mt. Bragg and Mt. Harper. We analysed 35 samples from Mt Bragg and Harper, and these range from 2.5 ka to 395 ka but with a significant number, especially at Mt Harper, yielding Holocene ages. The data show that the ice sheet thinned from at least 380 m above present ice with the majority of the samples deposited below 240 m above present ice (Fig. 4d and e) from the early to mid-Holocene. Thinning may have been underway at 17.6 ka but was certainly occurring progressively by 7.9 ka. The youngest age of 2.5 ka, close to present-day ice shows that present ice levels were reached by 2.5 ka. Samples from the boulder moraine on the sides

Table 2
Cosmogenic ^{10}Be and ^{26}Al surface exposure ages.

Sample ID	Alt. (m)	^{10}Be age[a] ± 1σ (int)[b] (ka)	±1σ (ext)[c] ^{10}Be (ka)	±1σ (full)[d] ^{10}Be (ka)	^{26}Al age[a] ± 1σ (int)[b] (ka)	±1σ (ext)[c] ^{26}Al (ka)	±1σ (full)[d] ^{26}Al (ka)	^{26}Al/^{10}Be ± 1σ	Regional ice surface[e](m)	Height above present ice[e] (m)
WIL-1	689	6.60 ± 0.29	0.64	0.83					550	139
WIL-3	722	5.91 ± 0.27	0.51	0.70					550	172
WIL-4	743	5.00 ± 0.46	0.60	0.73					550	193
WIL-5	746	7.87 ± 0.26	0.63	0.90	6.98 ± 0.47	0.89	1.0	6.36 ± 0.49	550	196
WIL-6	780	7.00 ± 0.47	0.72	0.89					550	230
WIL-8	572	6.21 ± 0.31	0.55	0.75					400	172
WIL-13	529	5.60 ± 0.22	0.49	0.66	5.17 ± 0.39	0.72	0.83	6.67 ± 0.58	400	129
WIL-15	500	7.02 ± 0.45	0.69	0.87					400	100
WIL-16	459	362 ± 12	33	46					400	59
WIL-17	442	5.22 ± 0.33	0.52	0.66					400	42
WIL-18	861	10.5 ± 0.4	0.9	1.3					575	286
WIL-19	841	6.41 ± 0.38	0.61	0.80					575	266
WIL-20	838	8.14 ± 0.31	0.73	0.99					575	263
WIL-21	831	9.70 ± 0.48	0.93	1.2					575	256
WIL-26	1055	8.85 ± 0.39	0.84	1.1					600	455
WIL-27	1055	572 ± 21	55	77					600	455
WIL-28	621	5.83 ± 0.35	0.57	0.74					500	121
WIL-31	665	111 ± 3	9	13					500	165
WIL-32	796	8.06 ± 0.36	0.69	0.96					500	296
WIL-33	795	6.99 ± 0.33	0.66	0.85					500	295
BRG-1	1048	19.7 ± 0.6	1.6	2.3					810	238
BRG-2	1047	14.0 ± 0.4	1.2	1.6					810	237
BRG-4	1049	7.86 ± 0.28	0.63	0.89					810	239
BRG-5	1002	206 ± 5	17	25					810	192
BRG-6	1000	41.1 ± 1.3	3.5	4.9					810	190
BRG-7	1000	74.0 ± 2.4	6.3	8.8					810	190
BRG-8	1000	37.0 ± 1.0	3.0	4.2					810	190
BRG-9	898	146 ± 4	12	17					810	88
BRG-10	900	158 ± 4	13	19					810	90
BRG-11	814	142 ± 3	12	17					810	4
BRG-13	1196	353 ± 8	31	44					813	383
BRG-14	1196	17.6 ± 0.6	1.5	2.1					813	383
BRG-15	1125	147 ± 3	12	17					813	312
BRG-16	1125	395 ± 9	35	50					813	312
BRG-19	1030	161 ± 4	14	19					813	217
BRG-20	1030	12.0 ± 0.4	1.0	1.4	11.5 ± 0.7	1.4	1.7	7.00 ± 0.47	813	217
BRG-21	920	149 ± 3	12	18					813	107
BRG-22	920	136 ± 4	12	16					813	107
BRG-23	870	286 ± 7	25	35					813	57
BRG-24	872	115 ± 4	10	14					813	59
BRG-25	842	209 ± 5	18	25					813	29
BRG-26	840	4.07 ± 0.19	0.39	0.53	3.73 ± 0.35	0.51	0.60	6.66 ± 0.64	813	27
BRG-27	816	2.51 ± 0.22	0.28	0.35					813	3
BRG-28	813	24.0 ± 0.7	2.0	2.8					813	0
HAR-1	878	4.44 ± 0.20	0.38	0.53	4.65 ± 0.39	0.64	0.75	7.56 ± 0.65	710	168
HAR-2	878	4.23 ± 0.18	0.36	0.51					710	168
HAR-3	878	3.14 ± 0.26	0.38	0.46					710	168
HAR-4	913	6.20 ± 0.23	0.56	0.74					710	203
HAR-5	913	5.70 ± 0.23	0.50	0.68	6.15 ± 0.40	0.71	0.87	7.73 ± 0.61	710	203
HAR-6	840	6.90 ± 0.30	0.62	0.82					710	130
HAR-7	840	7.62 ± 0.28	0.62	0.87	8.00 ± 0.50	1.0	1.2	7.47 ± 0.60	710	130
HAR-8	782	5.25 ± 0.21	0.43	0.59					710	72
HAR-9	780	34.0 ± 1.1	2.9	4.0					710	70
HAR-10	734	14.9 ± 0.6	1.3	1.8					710	24
HAR-11	734	9.71 ± 0.39	0.89	1.2					710	24

(*continued on next page*)

Table 2 (*continued*)

Sample ID	Alt. (m)	^{10}Be age[a] ± 1σ (int)[b] (ka)	±1σ (ext)[c] ^{10}Be (ka)	±1σ (full)[d] ^{10}Be (ka)	^{26}Al age[a] ± 1σ (int)[b] (ka)	±1σ (ext)[c] ^{26}Al (ka)	±1σ (full)[d] ^{26}Al (ka)	^{26}Al/^{10}Be ± 1σ	Regional ice surface[e](m)	Height above present ice[e] (m)
SCH-7	560	236 ± 8	21	29					300	260
SCH-10	874	1570 ± 53	190	280					300	574
SCH-11	876	3000 ± 151	550	860					300	576
SCH-13	829	677 ± 18	65	93					300	529
SCH-19	400	307 ± 10	28	39					300	100
SCH-20	401	289 ± 9	26	36					300	101
SCH-21	667	1560 ± 52	190	280					300	367
SCH-25	728	1120 ± 33	120	170					300	428
THO-1	730	865 ± 24	87	130					380	350
THO-3	782	813 ± 22	81	120	573 ± 40	91	110	4.74 ± 0.26	380	402
THO-5	840	953 ± 27	98	140	670 ± 49	110	140	4.68 ± 0.26	380	460
THO-7	465	40.4 ± 1.3	3.4	4.8					380	85
THO-8	465	24.9 ± 0.8	2.1	3.0					380	85
THO-9	465	29.0 ± 1.0	2.4	3.4	27.9 ± 1.6	3.4	4.1	6.94 ± 0.47	380	85
THO-10	465	28.8 ± 1.2	2.5	3.4	25.0 ± 1.5	3.0	3.7	6.21 ± 0.45	380	85
THO-11	520	51.1 ± 1.5	4.3	6.0					380	140
THO-12	530	32.5 ± 0.9	2.7	3.8					380	150
THO-13	414	36.0 ± 1.2	3.0	4.2					380	34
THO-14	414	28.1 ± 0.9	2.4	3.3					380	34
THO-15	414	12.8 ± 0.6	1.2	1.6	12.0 ± 0.8	1.5	1.8	6.82 ± 0.55	380	34
THO-16	414	23.0 ± 0.9	2.0	2.8	20.8 ± 1.2	2.6	3.1	6.50 ± 0.45	380	34
THO-17	410	45.6 ± 1.4	3.9	5.4					380	30
THO-18	410	28.7 ± 0.8	2.4	3.3					380	30
THO-19	410	380 ± 10	34	48					380	30
THO-20	410	310 ± 8	27	39					380	30
THO-21	545	563 ± 14	52	75	470 ± 31	70	85	5.54 ± 0.31	380	165
THO-24	635	96.0 ± 2.5	8.0	11	92.0 ± 5.1	11	14	6.74 ± 0.40	380	255
THO-25	480	173 ± 5	15	21					380	100
THO-26	477	188 ± 5	16	23					380	97
THO-27	477	29.7 ± 1.0	2.5	3.5					380	97
THO-28	475	33.8 ± 1.2	2.9	4.0					380	95
THN-7	570	546 ± 14	51	72					390	180
THN-8	570	603 ± 16	57	81					390	180
THN-10	515	4.56 ± 0.75	0.84	0.92	5.54 ± 0.40	0.68	0.81	8.78 ± 1.48	390	125
THN-12	390	51.4 ± 2.0	4.5	6.2					390	0
THN-13	390	81.9 ± 3.6	7.4	10					390	0
THN-15	435	72.5 ± 2.7	6.4	8.8					390	45
THN-17	463	46.0 ± 1.8	4.0	5.5					390	73
YAR-1	848	828 ± 22	82	120	603 ± 42	97	120	4.85 ± 0.27	560	288
YAR-2	850	897 ± 25	91	130					560	290
YAR-5	790	554 ± 14	51	73	487 ± 32	73	90	5.79 ± 0.32	560	230
YAR-7	768	730 ± 20	70	100					560	208
YAR-9	710	366 ± 9	32	46					560	150
YAR-11	690	255 ± 6	22	31					560	130
YAR-12	690	367 ± 9	32	46					560	130
YAR-14	670	630 ± 16	60	86					560	110
YAR-15	642	357 ± 9	31	45					610	32
YAR-16	644	540 ± 14	50	71					610	34
YAR-17	615	569 ± 14	53	76					610	5
YAR-18	615	696 ± 18	67	96					610	5

[a] Ages calculated with CRONUS-Earth CRONUScalc v.2.0 (Marrero et al., 2015), LSD scaling (Lifton et al., 2014), no erosion correction; attenuation length 153 ± 10 g cm^2; ^{26}Al and ^{10}Be production rates from CRONUS-Earth Project (Borchers et al., 2015).

[b] (int) = Internal uncertainties; includes only concentration uncertainties based on lab/AMS measurements.

[c] (ext) = External uncertainties; includes internal uncertainties plus scaling and production rate uncertainties.

[d] (full) = Full uncertainties; includes external uncertainties plus uncertainties on thickness (0.5 cm), pressure (10 hPa), attenuation length (10 g cm-2), and density (0.05 g cm^{-3}).

[e] Sample elevations are normalised to the elevation of the ice surface at the foot of the spur or peak on which the sample lies, and so the plots in Fig. 4 are in terms of elevation above present ice.

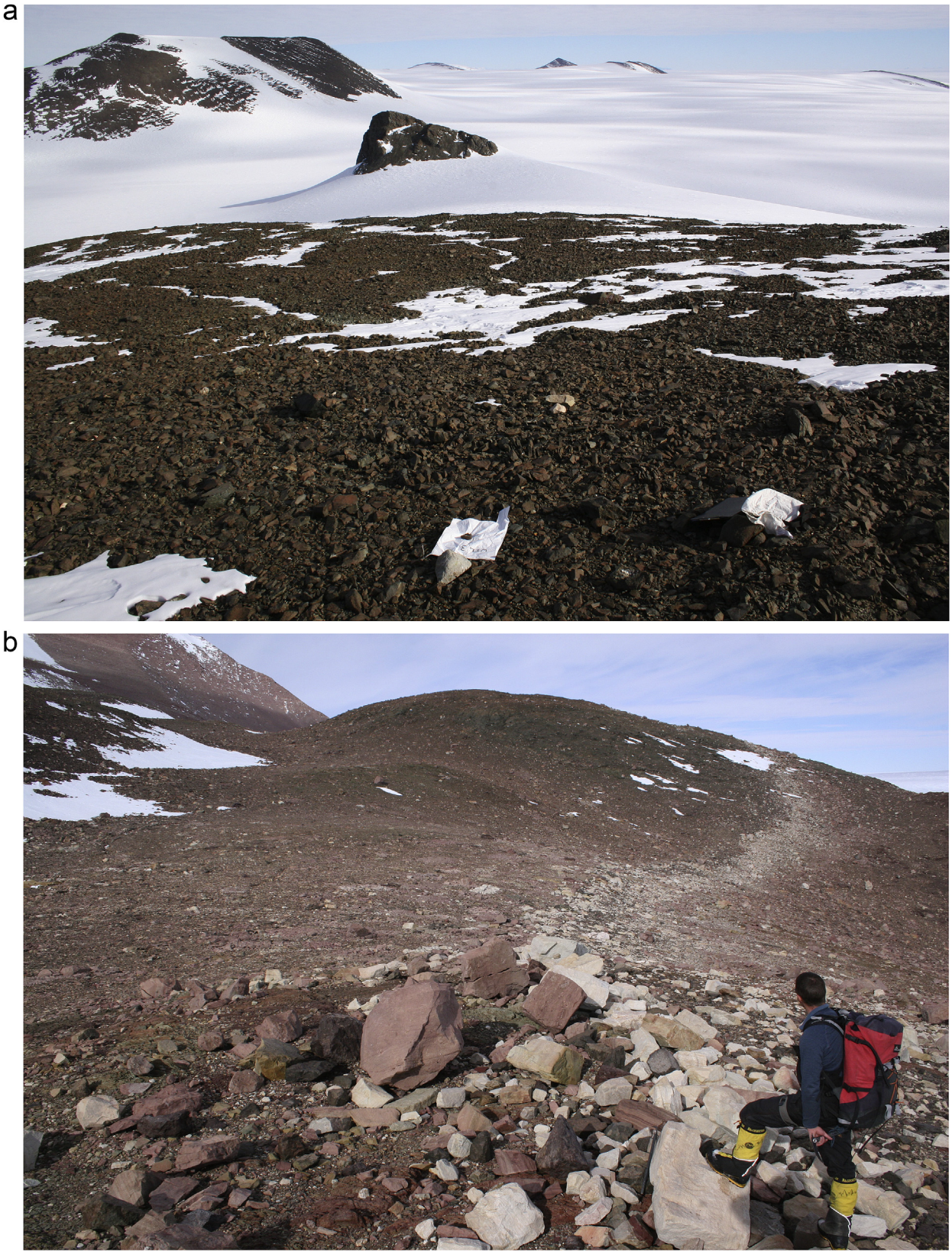

Fig. 3. Glacial geomorphology of the field area. (a) Erratic sandstone clasts on the Williams Hills, (b) Boulder limit on south flank of Mt. Bragg, Academy Glacier visible below, (c) Panorama of Sugden Ridge showing cross-cutting moraines: moraines deposited by an expanded Foundation Ice Stream slope down from R to L and moraines from an expanded MacNamara Glacier slope down from L to R. Red dots show samples, ^{10}Be ages in bold, and ^{26}Al ages in italics. Numbered black dots show elevations (m asl). (d) Striations on Pillow Knob, Williams Hills. A set of weathered, warm-based striations (parallel to compass-clinometer) are cut by a fresher set of cold-based striations that incise the weathered surface, trending top right to bottom left. (e) Weathered bedrock in the Schmidt Hills. (For interpretation of the references to colour in this figure legend, the reader is referred to the web version of this article.)

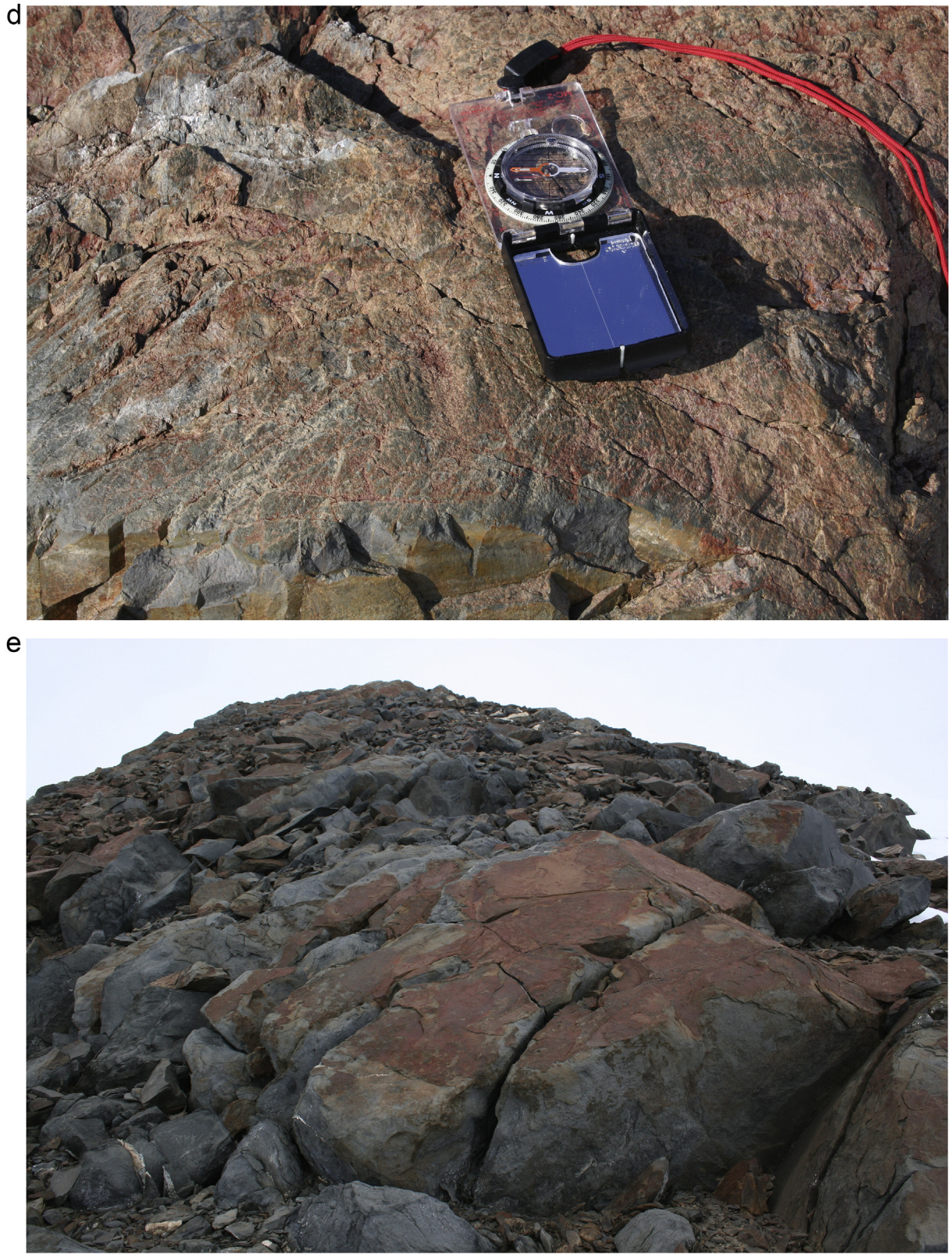

Fig. 3. (*continued*).

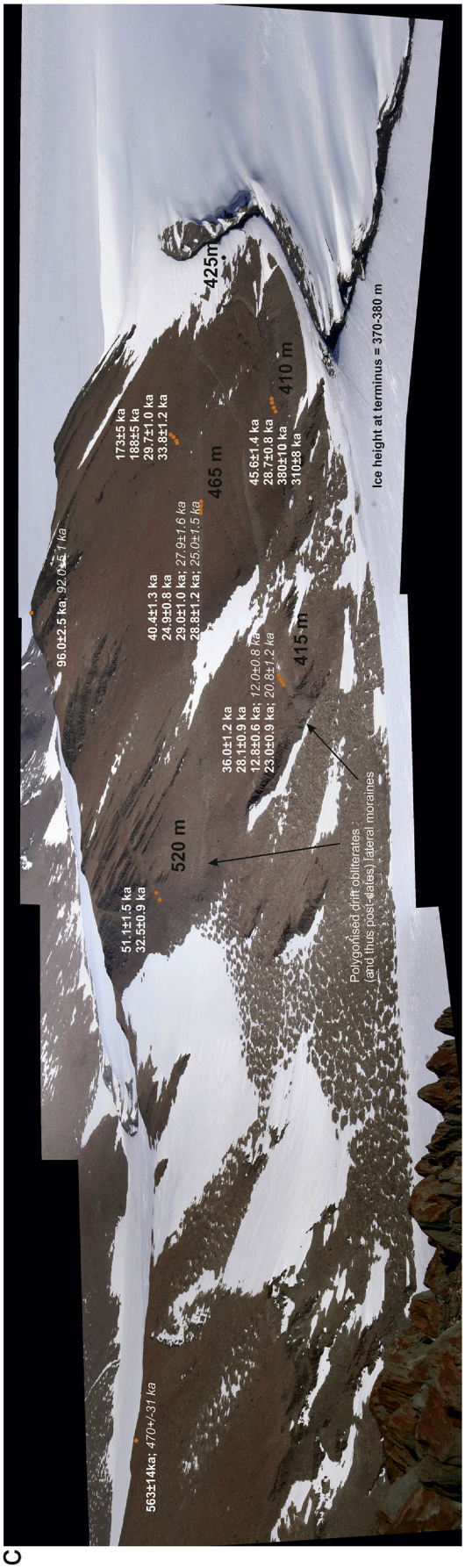

Fig. 3. (*continued*).

of Mt. Bragg (~200 m above present ice) yielded a mixed population of ages (12, 37, 41, 74, 161, 206 ka).

3.5.2.4. Thomas Hills. The 42 samples analysed from several nunataks along the Thomas Hills yield a range of ages with the majority dating from prior to the last glacial cycle, particularly on Mt. Yarborough and Clapperton Ridge (Fig. 4g–j), including ages up to 953 ka. However, two sites, Sugden Ridge and Bentley Peak, have erratic samples that yielded ages showing they were deposited during deglaciation from the Local Last Glacial Maximum (Fig. 4g). For example, one Holocene sample with an age of 4.2 ka occurs at 125 m above present ice on Bentley Peak, perched on fresh drift. This is consistent with the Bragg, Harper, and Williams massifs, to which it is most closely located. However, all other samples from the flanks of this site yield ages substantially older than the LGM and are likely reworked or have been preserved beneath ice. The ^{26}Al exposure ages on a subset of samples show discordant ages, implying a complex exposure history, and thus confirm this view of at least one period of burial.

3.5.2.5. Sugden Ridge. Sugden Ridge (Figs. 3c and 4g) yields a complex set of exposure ages on the cross-cutting moraines, and does not provide a clear thinning history for the Foundation Ice Stream. Each moraine has yielded a significant range of ages. The highest parts of Sugden Ridge yield pre-LGM exposure ages of 96 ka (peak) and 563 ka (col). The highest Foundation Ice Stream moraine yields ages of 51.1 and 32.5 ka. It is notable that all of the moraines below this yield mixed ages but that ages in the range 28–33 ka occur in every moraine. The most extensive and distinct moraine yields one age of 12.8 ka, which is the youngest age anywhere on this spur. The lowest elevation moraine provides mixed ages between 380 and 28.7 ka.

4. Discussion

The data reported here show that the Foundation Ice Stream and its tributary Academy Glacier thickened by 100s of metres during the LLGM. The data do not constrain the maximum thickening but it was >380–450 m close to the confluence of the Academy Glacier and the Foundation Ice Stream. The data do show progressive thinning during the Holocene, and this is consistent with recent data from Balco et al. (2016) that show similar thinning trajectories from the northern Pensacola Mountains (Fig. 3).

4.1. Foundation Ice Stream and Academy Glacier thinning histories

The most detailed thinning histories come from the north side of the Academy Glacier where the datasets from Williams Hills and Mt. Bragg and Mt. Harper give similar, but not identical, deglacial trajectories (Fig. 4f) of progressive thinning from the early-to mid-Holocene. Specifically the Williams Hills data have no samples younger than 5 ka whereas at Mt. Bragg and Mt. Harper there are younger samples. Moreover the rate of thinning may have been faster at Williams Hills than at Mt. Bragg/Mt. Harper (Fig. 4b, d, f). Mt. Hobbs, the highest summit of the Williams Hills, yielded an exposure age of 8.85 ka at 450 m above present ice. On Mt. Bragg, the highest sample taken, 383 m above present ice, yielded an age of 17.6 ka. The data do not directly constrain either the extent or timing of the maximum glaciation at either site.

The Williams Hills exposure ages are similar to the exposure ages reported from the same area by Balco et al. (2016), which also show progressive thinning through the first half of the Holocene and no ages <4.18 ka. Fig. 4b and f shows that the thinning trajectories of the two datasets are closely coincident. Farther south, in the Thomas Hills our data do not record a clear post-glacial

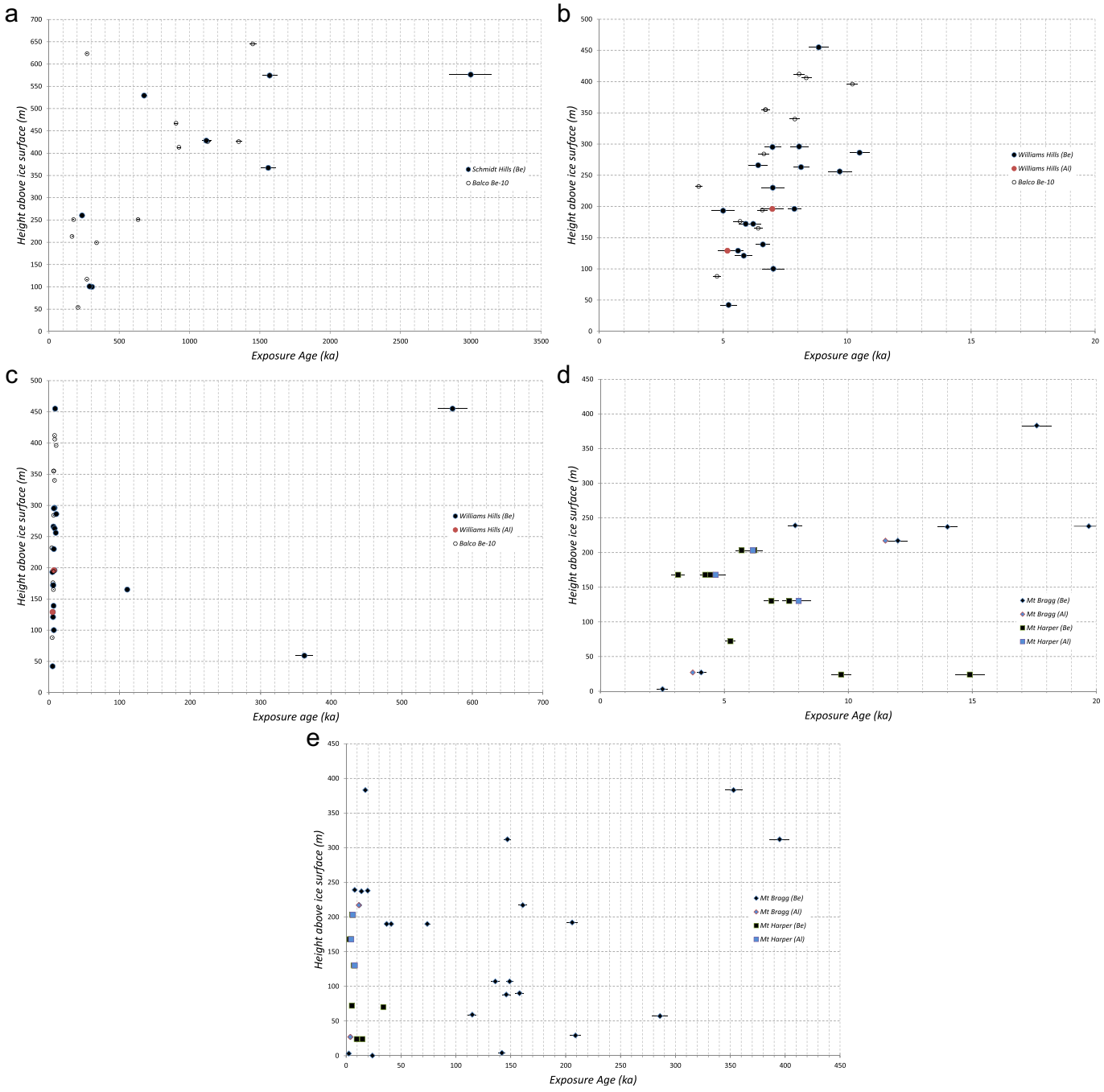

Fig. 4. Thinning histories of sites in the Pensacola Mountains. (a) Schmidt Hills (all samples), (b) Williams Hills (samples <20ka), (c) Williams Hills (all), (d) Mt. Bragg and Mt. Harper (<20 ka), (e) Mt. Bragg and Mt. Harper (all), (f) Combined dataset of Williams Hills, Mt. Bragg and Mt. Harper (<20ka), (g) Thomas Hills (Sugden Ridge, Clapperton Ridge, Bentley Peak) < 50 ka, (h) Thomas Hills (all), (i) Mt. Yarborough (<50 ka), (j) Mt. Yarborough (all). Data from this study as filled shapes, data from Balco et al. (2016) are plotted as open circles.

thinning trajectory apart from a single age of 4.2 ka at Bentley Peak and a single age of 12.8 ka amongst a mixed age population from a single moraine on Sugden Ridge. However, the dataset from Balco et al. (2016) show that ice was >250 m thicker at the southern end of the Thomas Hills in the early Holocene and that the ice thinned rapidly prior to 5 ka (Fig. 4i), consistent with the sites along the north side of the Academy Glacier.

4.2. Lack of recently exposed erratics in the Schmidt Hills

The lack of erratics younger than 236 ka in the Schmidt Hills, despite widespread evidence for LGM glaciation elsewhere in the Pensacola Mountains, is similar to the pattern found by Balco et al. (2016) from the same area, where all of the ^{10}Be apparent exposure ages in the Schmidt Hills were from prior to the last glacial cycle. Both our data and the data presented in Balco et al. (2016) show clear evidence for ice cover up to 450 m thicker than present in the Williams Hills, which lie only a few tens of kilometres south of the Schmidt Hills (Fig. 1), and so this difference is puzzling. Balco et al. (2016) undertook multiple isotopic analyses (^{10}Be, ^{21}Ne, ^{3}He, and ^{14}C) on their samples and showed that there were inconsistencies between the different isotopes. They argued that although their *in situ* ^{14}C apparent exposure ages showed a clear long-term exposure with no significant intervals of ice cover above 500 m elevation

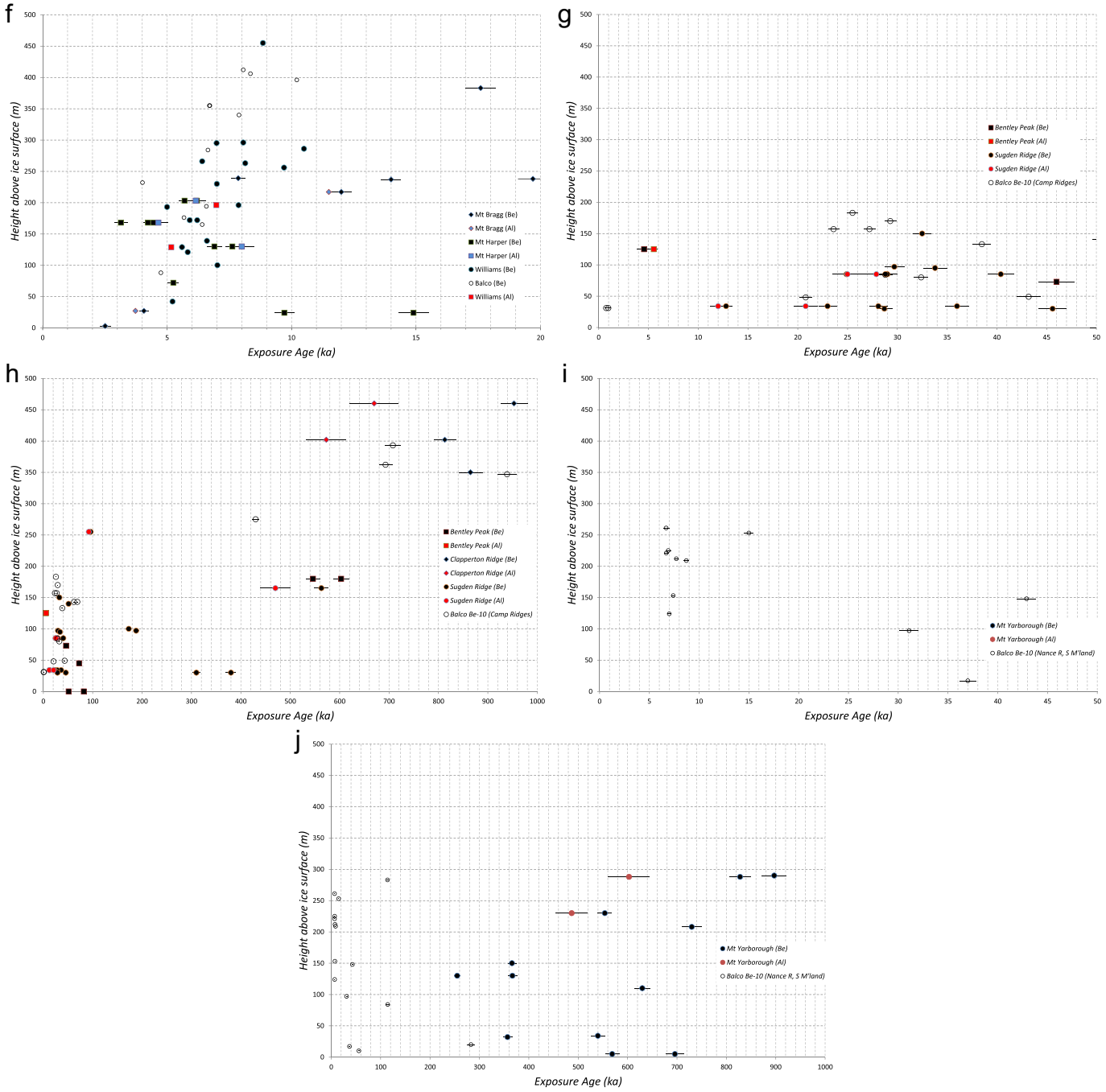

Fig. 4. (*continued*).

(corresponding to ice ~350 m thicker than present), the dataset could not be reconciled with simple Holocene thinning histories. They suggested that to explain the ages would require either significant unrecognized analytical errors (of up to 25%), or a complex and unlikely configuration of LGM ice, which transported the samples from prior exposure on higher summits in the Schmidt Hills. Balco et al. (2016) concluded that they could not clearly resolve the exposure history of the Schmidt Hills but that the *in situ* ^{14}C concentrations were clear in showing that any LGM ice cover of the area reached <500 m asl elevation.

We concur that the lack of dated evidence for LGM glaciation of the Schmidt Hills is difficult to explain. Perhaps it reflects some effect of lithology on analytical procedures or more probably an effect of patterns of local ice flow. It is notable that an expanded Childs Glacier, coming off the Iroquois plateau may have diverted the debris-bearing ice that was flowing NW over the Williams Hills to the west before it reached the Schmidt Hills (Fig. 1). The Balco et al. (2016) ^{14}C data require that the ice did not thicken more than ~350 m above present at the Schmidt Hills. Given that the Foundation Ice Stream thickened at least by 450 m only a few tens of km to the south then this would require a significant steepening of the Foundation Ice Stream gradient, or that the centreline of the Foundation Ice Stream thickened significantly more than the margins at Schmidt Hills (Balco et al., 2016). The implications of the Schmidt Hills data for former configuration of an expanded Foundation Ice Stream are explored further using a numerical flowband model in Whitehouse

et al. (2016), where it is demonstrated that differential thickening of the centre and margins of the Foundation Ice Stream could potentially explain the Schmidt Hills data.

4.3. Mixed age populations on boulder moraines and reworking of clasts

Conventionally, boulder moraines provide a useful fix on the position of a formerly expanded ice margin and rigorous dating of such a limit should yield a well-dated reconstruction of that margin. However, in the Pensacola Mountains we found that each of the boulder moraines we mapped and sampled (Mt. Bragg, Sugden Ridge) yielded mixed age populations. For this reason we have been unable to assign ages to any of the boulder moraines. Each of these boulder limits is associated with a present-day ice margin that is dominantly composed of blue-ice regions. The mixed ages imply that either the reworking of erratics along the blue-ice margins of Foundation Ice Stream may be pervasive, or that the debris has been emerging at the ice margin for millennia.

The cross-cutting moraines at Sugden Ridge reflect complex behaviour of the Foundation Ice Stream and locally-sourced MacNamara Glacier. There are a number of features of the mixed age populations of these moraines that are worthy of discussion. At face value, the mixed ages – ranging from 12.8 ka to 380 ka – are difficult to reconcile with the Williams/Bragg/Harper trajectory of an expanded Foundation Ice Stream at the LGM which thinned through the early to mid-Holocene. There are at least three possible explanations. Firstly, all fluctuations at Sugden Ridge predate the LLGM and have then been over-ridden by thicker LLGM ice. Overriding of landforms without modification by cold-based ice has been noted elsewhere in Antarctica (Sugden et al., 2005). In this case the youngest age of 12.8 ka may be the closest representative thinning age. Second, all fluctuations are post-LLGM but the majority of samples are reworked. This could explain the substantial scatter on every moraine sampled. Third, the data may reflect the real timing of fluctuations (dated by the youngest sample on each moraine) but would imply very small thickness changes at each site, and also ice sheet thickening that is inconsistent with the timing of ice sheet change elsewhere in the study area. The latter two explanations are very difficult to reconcile with the Bragg/Harper/Williams dataset and with evidence of the Foundation Ice Stream thinning by 125 m since 4.18 ka at Bentley Peak, and so we favour the first explanation, namely that the cross-cutting moraine sequences on Sugden Ridge have been over-ridden.

4.4. Comparison to other Weddell Sea deglacial chronologies

Our data can be compared with previous work on the glacial history of the Antarctic Ice Sheet in the Weddell Sea embayment. Bentley et al. (2010) showed modest LLGM thickening of 230–480 m in the southern Ellsworth Mountains followed by progressive thinning through the Holocene to reach present ice levels by c. 2 ka. This is similar to the glacial history reported here and both sites sit in similar configurations close to the present-day grounding line where thickening is likely to have been significant during past glacial periods. In the Shackleton Range, farther north along the Thiel Trough Ice Stream, Hein et al. (2011) showed that there had been minimal thickening at the LGM. The implication of this is that an expanded Thiel Trough Ice Stream could not have thickened significantly at the vicinity of the Shackleton Range (Hein et al., 2011; Hillenbrand et al., 2014). Ice core data from Berkner Island showed that this ice rise, with a current altitude of 886 m asl was not overridden by thick interior ice during the LGM and that it remained an independent ice centre throughout the last glacial cycle (Matsuoka et al., 2015; Mulvaney et al., 2007).

4.5. A late Holocene ice sheet readvance in the Weddell Sea?

Bradley et al. (2015) suggested that a number of puzzling glaciological and geophysical observations could be explained if the ice sheet in the Weddell Sea had retreated to smaller-than-present-limits in the mid-to Late Holocene and had subsequently advanced to its present configuration. Specifically, this would help explain observations of grounding lines existing in an apparently stable configuration on reverse slopes, and also low GPS-measured crustal uplift rates, including an observation of subsidence from at least one GPS receiver located in the interior of the ice sheet inboard of the grounding line. Moreover, a readvance from smaller-than-present would also explain the glaciological observations of significant Late Holocene flow re-organisation of the Institute and Möller Ice Streams (Siegert et al., 2013). Data from the Ellsworth Mountains are consistent with the concept of a Late Holocene ice sheet readvance since the youngest exposure ages of erratics close to the present margin are 2–3 thousand years old (Bentley et al., 2010; Hein et al., 2016a). Our new data from the Foundation Ice Stream are consistent with the data from the Ellsworth Mountains and glaciological observations from the Institute and Möller Ice Streams: specifically, in the Williams Hills there are no exposure ages younger than 5ka (our data) or 4 ka (Balco et al., 2016). Thus the ice margin in the vicinity of the Williams Hills may have thinned below present ice levels any time after 4ka, and only subsequently re-thickened. It is notable that the Williams Hills data show a very abrupt lower limit to exposure ages and that the data would be consistent with rapid ice sheet thinning adjacent to the Williams Hills at 4–5 ka. In the area of Mt. Bragg and Mt. Harper the youngest ages are slightly younger, with the youngest age above the present margin being 3.1 ka (an age at the present margin yields 2.5 ka but because it sits right at the present margin we cannot rule out it being reworked by the margin of a thickening ice sheet). In summary, our data are consistent with, but do not mandate, a scenario of Holocene thinning and subsequent thickening in the interval after 4 ka (Williams Hills) or 3.1–2.5 ka (Mt. Bragg/Mt. Harper).

4.6. Sampling of ice stream margins in Antarctica for thinning histories

In Antarctica, blue ice regions are regions of net ablation, often due to sublimation under katabatic wind regimes, in what would otherwise be the accumulation area of the ice sheet. They are a prime source of glacially-deposited material because ablation brings englacial material to the ice sheet surface. At face value, this makes them attractive areas for sampling for studies of former thinning histories. However, the problems of sampling for cosmogenic nuclide surface exposure dating from areas adjacent to blue ice moraines have been apparent in several studies and this is no exception. In areas adjacent to blue ice on the present-day Foundation Ice Stream or Academy Glacier, the apparent exposure ages we retrieved have a high component of scatter (e.g., Mt. Bragg, Sugden Ridge, Mt. Yarborough). As in several previous studies, the surface weathering characteristics or appearance of erratics cannot be used as a reliable guide to relative age: fresh-looking erratics regularly yield 'old' ages (see discussion in Balco (2011) and Hein et al. (2014)). Moreover, comparison of our work with that by Balco et al. (2016) shows that the proportion of younger ages can change markedly in closely adjacent sites: for example in the Thomas Hills we sampled Mt. Yarborough and found no samples younger than 255 ka ($n = 12$), yet sampling by Balco et al. of the adjacent nunataks on either side ('Nance Ridge' and 'South Mainland') yielded an age population where 50% of the ages were post-LGM in age ($n = 16$). This implies significant variations in spatial distribution.

This problem of complex exposure ages in blue-ice regions also applies to distinct geomorphological limits such as boulder moraines. Such a moraine can display a wide range of exposure ages, implying either reworking of old clasts and/or a long period of stability during which boulders were deposited. In the future, the complexity, once elaborated, holds potential for investigating the long-term stability of the ice sheet (Ackert et al., 2011; Hein et al., 2016a,b).

Balco et al. (2016) tried the screening approach suggested by Ackert et al. (2007) whereby faster, cheaper (but less accurate) ^{3}He analyses could be used to screen erratic populations for younger (post-LGM) clasts in a mixed population. Unfortunately in the Pensacola Mountains the erratic lithologies possessed unusual and variable He diffusion properties in quartz and so the ^{3}He analyses consistently underestimated exposure ages. In fact, Balco et al. (2016) concluded that the ^{3}He analyses simply acted as a proxy for diffusion properties of each lithology rather than any reliable measure of exposure age. *In situ* ^{14}C analyses have been used successfully in a small number of glacial geologic studies in Antarctica and elsewhere to test for clast recycling (e.g., White et al. (2011)). Balco et al. (2016) tried a similar approach in the Schmidt Hills to look at the reworking problem but the results suggest that there may be previously unrecognized analytical problems, and the data did not robustly constrain the reworking issue.

It is notable that in the Williams Hills - the area with least blue ice on the adjacent ice stream - both our study and that of Balco et al. (2016) yielded robust and closely similar thinning trajectories for post-LGM ice sheet behaviour. The implication is that recycling or inheritance is much less of a problem in this area and that the erratics can provide a robust age-elevation array.

5. Conclusions

A new dataset of geomorphological and cosmogenic nuclide surface exposure dating from the Pensacola Mountains allows us to make inferences on the deglacial history of this region, and in particular the deglacial history of the Foundation Ice Stream.

1 There is evidence of at least two glacial configurations: early warm-based glaciation(s) that weathering suggests was/were relatively old, and second, more recent cold-based glaciation(s).
2 The geomorphology of the area records a thinning history since the local Last Glacial Maximum.
3 Thickening in the most recent glaciation was at least 450 m in Williams Hills and at least 380 m on Mt. Bragg.
4 The timing of the onset of thinning is not well-constrained by these data but was well underway by the Early Holocene.
5 Cosmogenic isotopic data show that there was progressive thinning of the Foundation Ice Stream and the tributary Academy Glacier between 10 and 2.5ka. The thinning trajectory is similar at multiple sites: three sites on the flanks of the Foundation Ice Stream/Academy Glacier, from two independent studies, show a consistent thinning history, reaching present ice levels by 2.5ka.
6 Geomorphology and dating in the Thomas Hills shows thickening occurred, but has also revealed a complex interaction between the Foundation Ice Stream margin and local ice. These fluctuations are not yet well dated.
7 The modest thinning history reported here is broadly similar to that from the Ellsworth Mountains (Bentley et al., 2010; Hein et al., 2016a).
8 The thinning history at this and other sites is consistent with, but does not mandate, a retreat of the grounding line behind the present ice sheet margin followed by a Late Holocene readvance (Bradley et al., 2015).
9 Clasts with complex exposure histories are pervasive, as in most blue ice areas of Antarctica, but also highly variable over short distances.
10 These data provide constraints on attempts to infer former ice sheet extent in the Weddell Sea using numerical flowband modelling of the former Thiel Trough Ice Stream (Whitehouse et al., 2016).

Acknowledgements

We thank the British Antarctic Survey pilots and operations staff who facilitated the work in the Pensacola Mountains. Particular thanks to James Wake for his assistance in the field. The work reported here forms part of NERC grants NE/F014260/1, NE/F014252/1, and NE/F014228/1. We thank Greg Balco and a second, anonymous reviewer for their comments, which improved the paper.

References

Ackert Jr., R.P., Mukhopadhyay, S., Pollard, D., DeConto, R.M., Putnam, A.E., Borns Jr., H.W., 2011. West Antarctic Ice Sheet elevations in the Ohio Range: geologic constraints and ice sheet modeling prior to the last highstand. Earth Planet. Sci. Lett. 307, 83–93.
Ackert, R.P., Mukhopadhyay, S., Parizek, B.R., Borns, H.W., 2007. Ice elevation near the west Antarctic ice sheet divide during the last glaciation. Geophys. Res. Lett. 34.
Atkins, C.B., Barrett, P.J., Hicock, S.R., 2002. Cold glaciers erode and deposit: evidence from allan Hills, Antarctica. Geology 30, 659–662.
Balco, G., 2011. Contributions and unrealized potential contributions of cosmogenic-nuclide exposure dating to glacier chronology, 1990-2010. Quat. Sci. Rev. 30, 3–27.
Balco, G., Todd, C., Huybers, K., Campbell, S., Vermuelen, M., Hegland, M., Goehring, B.M., Hillebrand, T.R., 2016. Cosmogenic-nuclide exposure ages from the Pensacola mountains adjacent to the foundation ice stream, Antarctica. Am. J. Sci. 316.
Bentley, M.J., 2010. The Antarctic palaeo record and its role in improving predictions of future Antarctic Ice Sheet change. J. Quat. Sci. 25, 5–18.
Bentley, M.J., Fogwill, C.J., Kubik, P.W., Sugden, D.E., 2006. Geomorphological evidence and cosmogenic Be-10/Al-26 exposure ages for the last glacial maximum and deglaciation of the Antarctic Peninsula ice sheet. Geol. Soc. Am. Bull. 118, 1149–1159.
Bentley, M.J., Fogwill, C.J., Le Brocq, A.M., Hubbard, A.L., Sugden, D.E., Dunai, T.J., Freeman, S., 2010. Deglacial history of the west Antarctic ice sheet in the Weddell sea embayment: constraints on past ice volume change. Geology 38, 411–414.
Bentley, M.J., Ó Cofaigh, C., Anderson, J.B., Conway, H., Davies, B., Graham, A.G.C., Hillenbrand, C.-D., Hodgson, D.A., Jamieson, S.S.R., Larter, R.D., Mackintosh, A., Smith, J.A., Verleyen, E., Ackert, R.P., Bart, P.J., Berg, S., Brunstein, D., Canals, M., Colhoun, E.A., Crosta, X., Dickens, W.A., Domack, E., Dowdeswell, J.A., Dunbar, R., Ehrmann, W., Evans, J., Favier, V., Fink, D., Fogwill, C.J., Glasser, N.F., Gohl, K., Golledge, N.R., Goodwin, I., Gore, D.B., Greenwood, S.L., Hall, B.L., Hall, K., Hedding, D.W., Hein, A.S., Hocking, E.P., Jakobsson, M., Johnson, J.S., Jomelli, V., Jones, R.S., Klages, J.P., Kristoffersen, Y., Kuhn, G., Leventer, A., Licht, K., Lilly, K., Lindow, J., Livingstone, S.J., Massé, G., McGlone, M.S., McKay, R.M., Melles, M., Miura, H., Mulvaney, R., Nel, W., Nitsche, F.O., O'Brien, P.E., Post, A.L., Roberts, S.J., Saunders, K.M., Selkirk, P.M., Simms, A.R., Spiegel, C., Stolldorf, T.D., Sugden, D.E., van der Putten, N., van Ommen, T., Verfaillie, D., Vyverman, W., Wagner, B., White, D.A., Witus, A.E., Zwartz, D., 2014. A community-based geological reconstruction of Antarctic ice sheet deglaciation since the last glacial maximum. Quat. Sci. Rev. 100, 1–9.
Bierman, P.R., Caffee, M.W., Davis, P.T., Marsella, K., Pavich, M., Colgan, P., Mickelson, D., Larsen, J., 2002. Rates and timing of earth surface processes from in situ- produced cosmogenic Be-10, Beryllium. Mineral. Petrol. Geochem. 147–205.
Borchers, B., Marrero, S., Balco, G., Caffee, M., Goehring, B., Lifton, N., Nishiizumi, K., Phillips, F., Schaefer, J., Stone, J., 2015. Geological calibration of spallation production rates in the CRONUS-Earth project. Quat. Geochronol. 31, 188–198.
Bradley, S.L., Hindmarsh, R.C.A., Whitehouse, P.L., Bentley, M.J., King, M.A., 2015. Low post-glacial rebound rates in the Weddell Sea due to Late Holocene ice-sheet readvance. Earth Planet. Sci. Lett. 413, 79–89.
Clark, P.U., Dyke, A.S., Shakun, J.D., Carlson, A.E., Clark, J., Wohlfarth, B., Mitrovica, J.X., Hostetler, S.W., McCabe, A.M., 2009. The last glacial maximum. Science 325, 710–714.
Fretwell, P., Pritchard, H.D., Vaughan, D.G., Bamber, J.L., Barrand, N.E., Bell, R., Bianchi, C., Bingham, R.G., Blankenship, D.D., Casassa, G., Catania, G., Callens, D., Conway, H., Cook, A.J., Corr, H.F.J., Damaske, D., Damm, V., Ferraccioli, F.,

Forsberg, R., Fujita, S., Gim, Y., Gogineni, P., Griggs, J.A., Hindmarsh, R.C.A., Holmlund, P., Holt, J.W., Jacobel, R.W., Jenkins, A., Jokat, W., Jordan, T., King, E.C., Kohler, J., Krabill, W., Riger-Kusk, M., Langley, K.A., Leitchenkov, G., Leuschen, C., Luyendyk, B.P., Matsuoka, K., Mouginot, J., Nitsche, F.O., Nogi, Y., Nost, O.A., Popov, S.V., Rignot, E., Rippin, D.M., Rivera, A., Roberts, J., Ross, N., Siegert, M.J., Smith, A.M., Steinhage, D., Studinger, M., Sun, B., Tinto, B.K., Welch, B.C., Wilson, D., Young, D.A., Xiangbin, C., Zirizzotti, A., 2013. Bedmap2: improved ice bed, surface and thickness datasets for Antarctica. Cryosphere 7, 375–393.

Harig, C., Simons, F.J., 2015. Accelerated West Antarctic ice mass loss continues to outpace East Antarctic gains. Earth Planet. Sci. Lett. 415, 134–141.

Hein, A.S., Fogwill, C.J., Sugden, D.E., Xu, S., 2011. Glacial/interglacial ice-stream stability in the Weddell Sea embayment, Antarctica. Earth Planet. Sci. Lett. 307, 211–221.

Hein, A.S., Fogwill, C.J., Sugden, D.E., Xu, S., 2014. Geological scatter of cosmogenic-nuclide exposure ages in the Shackleton Range, Antarctica: implications for glacial history. Quat. Geochronol. 19, 52–66.

Hein, A.S., Marrero, S.M., Woodward, J., Dunning, S.A., Winter, K., Westoby, M.J., Freeman, S.P.H.T., Shanks, R.P., Sugden, D.E., 2016a. Mid-holocene pulse of thinning in the Weddell sea sector of the west Antarctic ice sheet. Nat. Commun. 7. Article no 12511.

Hein, A.S., Woodward, J., Marrero, S.M., Dunning, S.A., Steig, E.J., Freeman, S.P.H.T., Stuart, F.M., Winter, K., Westoby, M.J., Sugden, D.E., 2016b. Evidence for the stability of the west Antarctic ice sheet divide for 1.4 million years. Nat. Commun. 7. Article no 10325.

Hellmer, H.H., Kauker, F., Timmermann, R., Determann, J., Rae, J., 2012. Twenty-first-century warming of a large Antarctic ice-shelf cavity by a redirected coastal current. Nature 485, 225–228.

Hillenbrand, C.-D., Bentley, M.J., Stolldorf, T.D., Hein, A.S., Kuhn, G., Graham, A.G.C., Fogwill, C.J., Kristoffersen, Y., Smith, J.A., Anderson, J.B., Larter, R.D., Melles, M., Hodgson, D.A., Mulvaney, R., Sugden, D.E., 2014. Reconstruction of changes in the Weddell sea sector of the Antarctic ice sheet since the last glacial maximum. Quat. Sci. Rev. 100, 111–136.

Hillenbrand, C.-D., Melles, M., Kuhn, G., Larter, R.D., 2012. Marine geological constraints for the grounding-line position of the Antarctic ice sheet on the southern Weddell sea shelf at the last glacial maximum. Quat. Sci. Rev. 32, 25–47.

Hodgson, D.A., Bentley, M.J., 2013. Lake highstands in the Pensacola Mountains and Shackleton range 4300-2250 cal. yr BP: evidence of a warm climate anomaly in the interior of Antarctica. Holocene 23, 388–397.

Joughin, I., Bamber, J.L., 2005. Thickening of the ice stream catchments feeding the Filchner-Ronne Ice Shelf, Antarctica. Geophys. Res. Lett. 32.

King, M.A., Bingham, R.J., Moore, P., Whitehouse, P.L., Bentley, M.J., Milne, G.A., 2012. Lower satellite-gravimetry estimates of Antarctic sea-level contribution. Nature 491, 586-+.

Kohl, C.P., Nishiizumi, K., 1992. Chemical Isolation of quartz for measurement of Insitu-produced cosmogenic nuclides. Geochim. Cosmochim. Acta 56, 3583–3587.

Lal, D., 1991. Cosmic-ray labeling of erosion surfaces - in situ nuclide production-rates and erosion models. Earth Planet. Sci. Lett. 104, 424–439.

Larter, R.D., Graham, A.G.C., Hillenbrand, C.-D., Smith, J.A., Gales, J.A., 2012. Late Quaternary grounded ice extent in the Filchner Trough, Weddell Sea, Antarctica: new marine geophysical evidence. Quat. Sci. Rev. 53, 111–122.

Le Brocq, A.M., Bentley, M.J., Hubbard, A., Fogwill, C.J., Sugden, D.E., Whitehouse, P.L., 2011. Reconstructing the Last Glacial Maximum ice sheet in the Weddell Sea embayment, Antarctica, using numerical modelling constrained by field evidence. Quat. Sci. Rev. 30, 2422–2432.

Lifton, N., Sato, T., Dunai, T.J., 2014. Scaling in situ cosmogenic nuclide production rates using analytical approximations to atmospheric cosmic-ray fluxes. Earth Planet. Sci. Lett. 386, 149–160.

Mackintosh, A., Golledge, N., Domack, E., Dunbar, R., Leventer, A., White, D., Pollard, D., DeConto, R., Fink, D., Zwartz, D., Gore, D., Lavoie, C., 2011. Retreat of the East Antarctic ice sheet during the last glacial termination. Nat. Geosci. 4, 195–202.

Marrero, S., Phillips, F.M., Borchers, B., Lifton, N., Aumer, R., Balco, G., 2015. Cosmogenic nuclide systematics and the CRONUScalc Program. Quat. Geochronol. 31, 160–187. CRONUS-Earth Special Volume.

Matsuoka, K., Hindmarsh, R.C.A., Moholdt, G., Bentley, M.J., Pritchard, H.D., Brown, J., Conway, H., Drews, R., Durand, G., Goldberg, D., Hattermann, T., Kingslake, J., Lenaerts, J.T.M., Martín, C., Mulvaney, R., Nicholls, K.W., Pattyn, F., Ross, N., Scambos, T., Whitehouse, P.L., 2015. Antarctic ice rises and rumples: their properties and significance for ice-sheet dynamics and evolution. Earth-Sci. Rev. 150, 724–745.

Mulvaney, R., Arrowsmith, C., Barnola, J., McCormack, T., Loulergue, L., Raynaud, D., Lipenkov, V., Hindmarsh, R., 2007. A deglaciation climate and ice sheet history of the Weddell Sea region from the Berkner Island ice core. Quat. Int. 167–168, 294–295.

Nishiizumi, K., 2004. Preparation of Al-26 AMS standards. Nucl. Instrum. Methods Phys. Res. Sect. B-Beam Interact. Mater. Atoms 223–24, 388–392.

Nishiizumi, K., Imamura, M., Caffee, M.W., Southon, J.R., Finkel, R.C., McAninch, J., 2007. Absolute calibration of Be-10 AMS standards. Nucl. Instrum. Methods Phys. Res. Sect. B-Beam Interact. Mater. Atoms 258, 403–413.

Ross, N., Bingham, R.G., Corr, H.F.J., Ferraccioli, F., Jordan, T.A., Le Brocq, A., Rippin, D.M., Young, D., Blankenship, D.D., Siegert, M.J., 2012. Steep reverse bed slope at the grounding line of the Weddell Sea sector in West Antarctica. Nat. Geosci. 5, 393–396.

Schmidt, D.L., Williams, P.L., Nelson, W.H., 1978. In: Reston, V.A. (Ed.), Geologic Map of the Schmidt Hills Quadrangle and Part of the Gambacorta Peak Quadrangle, Pensacola Mountains, Antarctica, Antarctic Map.

Schoof, C., 2007. Ice sheet grounding line dynamics: steady states, stability, and hysteresis. J. Geophys. Res.-Earth Surf. 112.

Shepherd, A., Ivins, E.R., Geruo, A., Barletta, V.R., Bentley, M.J., Bettadpur, S., Briggs, K.H., Bromwich, D.H., Forsberg, R., Galin, N., Horwath, M., Jacobs, S., Joughin, I., King, M.A., Lenaerts, J.T.M., Li, J.L., Ligtenberg, S.R.M., Luckman, A., Luthcke, S.B., McMillan, M., Meister, R., Milne, G., Mouginot, J., Muir, A., Nicolas, J.P., Paden, J., Payne, A.J., Pritchard, H., Rignot, E., Rott, H., Sorensen, L.S., Scambos, T.A., Scheuchl, B., Schrama, E.J.O., Smith, B., Sundal, A.V., van Angelen, J.H., van de Berg, W.J., van den Broeke, M.R., Vaughan, D.G., Velicogna, I., Wahr, J., Whitehouse, P.L., Wingham, D.J., Yi, D.H., Young, D., Zwally, H.J., 2012. A reconciled estimate of ice-sheet mass balance. Science 338, 1183–1189.

Siegert, M., Ross, N., Corr, H., Kingslake, J., Hindmarsh, R., 2013. Late Holocene ice-flow reconfiguration in the Weddell sea sector of west Antarctica. Quat. Sci. Rev. 78, 98–107.

Stone, J.O., 2000. Air pressure and cosmogenic isotope production. J. Geophys. Res.-Solid Earth 105, 23753–23759.

Suganuma, Y., Miura, H., Zondervan, A., Okuno, J., 2014. East Antarctic deglaciation and the link to global cooling during the Quaternary: evidence from glacial geomorphology and Be-10 surface exposure dating of the Sor Rondane Mountains, Dronning Maud Land. Quat. Sci. Rev. 97, 102–120.

Sugden, D.E., Balco, G., Cowdery, S.G., Stone, J.O., Sass, L.C., 2005. Selective glacial erosion and weathering zones in the coastal mountains of Marie Byrd Land, Antarctica. Geomorphology 67, 317–334.

Velicogna, I., Sutterley, T.C., van den Broeke, M.R., 2014. Regional acceleration in ice mass loss from Greenland and Antarctica using GRACE time-variable gravity data. Geophys. Res. Lett. 41, 8130–8137.

White, D., Fueloep, R.-H., Bishop, P., Mackintosh, A., Cook, G., 2011. Can in-situ cosmogenic (14)C be used to assess the influence of clast recycling on exposure dating of ice retreat in Antarctica? Quat. Geochronol. 6, 289–294.

Whitehouse, P.L., Bentley, M.J., Le Brocq, A.M., 2012. A deglacial model for Antarctica: geological constraints and glaciological modelling as a basis for a new model of Antarctic glacial isostatic adjustment. Quat. Sci. Rev. 32, 1–24.

Whitehouse, P.L., Bentley, M.J., Vieli, A., Jamieson, S.S.R., Hein, A.S., Sugden, D.E., 2016. Controls on last glacial maximum ice expansion in the Weddell sea embayment. Antarctica. J. Geophys. Res.-Earth Surf. http://dx.doi.org/10.1002/2016JF004121.

Williams, S.D.P., Moore, P., King, M.A., Whitehouse, P.L., 2014. Revisiting grace Antarctic ice mass trends and accelerations considering autocorrelation. Earth Planet. Sci. Lett. 385, 12–21.

Wright, A.P., Le Brocq, A.M., Cornford, S.L., Bingham, R.G., Corr, H.F.J., Ferraccioli, F., Jordan, T.A., Payne, A.J., Rippin, D.M., Ross, N., Siegert, M.J., 2014. Sensitivity of the Weddell Sea sector ice streams to sub-shelf melting and surface accumulation. Cryosphere 8, 2119–2134.

Xu, S., Dougans, A.B., Freeman, S., Schnabel, C., Wilcken, K.M., 2010. Improved Be-10 and Al-26-AMS with a 5 MV spectrometer. Nucl. Instrum. Methods Phys. Res. Sect. B-Beam Interact. Mater. Atoms 268, 736–738.

Xu, S., Freeman, S.P.H.T., Rood, D.H., Shanks, R.P., 2014. Al-26 interferences in accelerator mass spectrometry measurements. Nucl. Instrum. Methods Phys. Res. Sect. B-Beam Interact. Mater. Atoms 333, 42–45.

Xu, S., Freeman, S.P.H.T., Sanderson, D., Shanks, R.P., Wilcken, K.M., 2013. Cl can interfere with Al3+ AMS but B need not matter to Be measurement. Nucl. Instrum. Methods Phys. Res. Sect. B-Beam Interact. Mater. Atoms 294, 403–405.